Published Online: 6 September, 2019 | Supp Info: http://doi.org/10.1084/jem.20180371
Downloaded from jem.rupress.org on September 19, 2019

JEM Journal of Experimental Medicine

ARTICLE

Cytosolic PCNA interacts with p47phox and controls NADPH oxidase NOX2 activation in neutrophils

Delphine Ohayon[1,2*], Alessia De Chiara[1,2*], Pham My-Chan Dang[2,3], Nathalie Thieblemont[1,2], Simon Chatfield[1,2], Viviana Marzaioli[2,3], Sabrina Sofia Burgener[4,5], Julie Mocek[1,2], Céline Candalh[1,2], Coralie Pintard[2,3], Pascale Tacnet-Delorme[6], Gilles Renault[1,2], Isabelle Lagoutte[1,2], Maryline Favier[1,2], Francine Walker[7], Margarita Hurtado-Nedelec[2,3], Dominique Desplancq[8], Etienne Weiss[8], Charaf Benarafa[4,5], Dominique Housset[6], Jean-Claude Marie[2,3], Philippe Frachet[6], Jamel El-Benna[2,3], and Véronique Witko-Sarsat[1,2]

Neutrophils produce high levels of reactive oxygen species (ROS) by NADPH oxidase that are crucial for host defense but can lead to tissue injury when produced in excess. We previously described that proliferating cell nuclear antigen (PCNA), a nuclear scaffolding protein pivotal in DNA synthesis, controls neutrophil survival through its cytosolic association with procaspases. We herein showed that PCNA associated with p47phox, a key subunit of NADPH oxidase, and that this association regulated ROS production. Surface plasmon resonance and crystallography techniques demonstrated that the interdomain-connecting loop of PCNA interacted directly with the phox homology (PX) domain of the p47phox. PCNA inhibition by competing peptides or by T2AA, a small-molecule PCNA inhibitor, decreased NADPH oxidase activation in vitro. Furthermore, T2AA provided a therapeutic benefit in mice during trinitro-benzene-sulfonic acid (TNBS)–induced colitis by decreasing oxidative stress, accelerating mucosal repair, and promoting the resolution of inflammation. Our data suggest that targeting PCNA in inflammatory neutrophils holds promise as a multifaceted antiinflammatory strategy.

Introduction

Neutrophils are key cells of the innate immune system (Mantovani et al., 2011) but may also be involved in pathological inflammatory processes when their activation and elimination are not properly regulated (Soehnlein et al., 2017). At sites of inflammation, neutrophils release biological molecules including proteases and ROS that can kill pathogens but also cause host tissue damage (Nauseef, 2007). The enzyme responsible for ROS production in neutrophils is the phagocyte NADPH oxidase (NOX2), a complex composed of two membrane proteins (gp91phox, p22phox) and four cytosolic proteins (p47phox, p67phox, p40phox, and the small GTPase Rac1/2) that assemble upon activation (El-Benna et al., 2016). Although ROS production is important for innate immunity, excessive ROS release can induce oxidative stress, leading to cell death and tissue injury (Nathan and Cunningham-Bussel, 2013). ROS are involved in numerous inflammatory diseases such as rheumatoid arthritis, inflammatory bowel disease, atherosclerosis, and aging (Lambeth et al., 2008). Coordination between neutrophil activation, ROS production, and cell death is pivotal in both host defense and the control of inflammation (Kennedy and DeLeo, 2009; Geering and Simon, 2011).

In this context, we have previously shown that the proliferating cell nuclear antigen (PCNA) protein plays a key role in neutrophil apoptosis (Witko-Sarsat et al., 2010; Ohayon et al., 2016). In the majority of cell types, PCNA is an exclusively nuclear protein that regulates processes related to DNA replication including cell cycle regulation and recombination (Maga and Hubscher, 2003). It has been dubbed the "maestro of the replication fork" (Moldovan et al., 2007). PCNA exists as a homotrimer that encircles duplex DNA, forming a ring-shaped clamp. PCNA is a trimer, and each monomer is composed of two similarly folded globular regions linked by a flexible interdomain-connecting loop, which is the preferred site for the binding of partner molecules (Warbrick, 1998). PCNA is a scaffolding

[1]Institut National de la Santé et de la Recherche Médicale U1016, Centre National de la Recherche Scientifique UMR 8104, Université Paris-Descartes, Cochin Institute, Paris, France; [2]LabEx Inflamex, Sorbonne Paris Cité, Paris, France; [3]Institut National de la Santé et de la Recherche Médicale U1149, Centre National de la Recherche Scientifique ERL8252, Centre de Recherche sur l'Inflammation, Université Paris Diderot, Faculté de Médecine, Site Xavier Bichat, Paris, France; [4]Institute of Virology and Immunology, Mittelhäusern, Switzerland; [5]Department of Infectious Diseases and Pathobiology, Vetsuisse Faculty, University of Bern, Bern, Switzerland; [6]Université Grenoble Alpes, Commissariat à l'Énergie Atomique et aux Énergies Alternatives, Centre National de la Recherche Scientifique, Institut de Biologie Structurale, Grenoble, France; [7]Department of Pathology, Bichat Hospital, Paris, France; [8]Ecole Supérieure de Biotechnologie de Strasbourg, Centre National de la Recherche Scientifique UMR 7242, Université de Strasbourg, Strasbourg, France.

*D. Ohayon and A. De Chiara contributed equally to this paper; Correspondence to Véronique Witko-Sarsat: veronique.witko@inserm.fr.

© 2019 Ohayon et al. This article is distributed under the terms of an Attribution–Noncommercial–Share Alike–No Mirror Sites license for the first six months after the publication date (see http://www.rupress.org/terms/). After six months it is available under a Creative Commons License (Attribution–Noncommercial–Share Alike 4.0 International license, as described at https://creativecommons.org/licenses/by-nc-sa/4.0/).

protein and has no intrinsic enzymatic activity. Reflecting the wide variety of roles of PCNA, >100 PCNA-interacting proteins involved in DNA-related processes have been identified (Maga and Hubscher, 2003).

In mature neutrophils, on the other hand, PCNA is expressed exclusively in the cytosol. PCNA is exported from the nucleus at the end of granulocytic differentiation via a nuclear export sequence we have previously identified (Bouayad et al., 2012). PCNA dictates neutrophil survival by binding to apoptotic procaspases, sequestering and preventing their activation (Witko-Sarsat et al., 2010). Neutrophils are fully differentiated nonproliferative cells, suggesting the cytosolic PCNA may coordinate functions apart from those related to proliferation. Cytosolic PCNA also promotes survival in acute myeloid leukemic cells resistant to chemotherapy. Furthermore, PCNA promotes glycolysis in these cells, serving as a scaffold for glycolytic proteins (Ohayon et al., 2016), promoting cell functionality in addition to restraining apoptosis. Whether PCNA has other binding partners in the cytosol of neutrophils and what contribution PCNA makes to neutrophil function more broadly remains poorly understood (Witko-Sarsat and Ohayon, 2016).

Given these roles of PCNA as a scaffold, we performed an exploratory proteomic analysis testing for novel PCNA partners within the neutrophil cytosol. We show using a number of techniques that PCNA associates with p47phox, a key subunit of the NADPH oxidase complex, and that this association regulates ROS production. Interfering with this association resulted in a potent in vivo antiinflammatory effect in two neutrophil-dominated models of inflammation, zymosan-induced peritonitis and trinitro-benzene-sulfonic acid (TNBS)–induced colitis.

Results

Cytosolic PCNA interacts with the phox homology (PX) domain of p47phox

We identified PCNA partners by coimmunoprecipitation and mass spectrometry (MS) analysis. PCNA was associated with proteins involved in cytoskeleton function, oxidant regulation, cell signaling, and glycolysis, as previously described in HL-60 cells (Ohayon et al., 2016; Table 1). Notably, the cytosolic components of the NADPH oxidase/NOX2, namely p47phox, p67phox, and p40phox as well as kinases and GTP-binding proteins, were associated with PCNA, suggesting a potential role of PCNA in the modulation of NADPH oxidase activity. As p47phox, p67phox, and p40phox form a complex in the cytosol, we examined the individual in vitro interactions between recombinant PCNA and p47phox, p67phox, p40phox, and Rac2 by surface plasmon resonance (SPR). A strong interaction was observed between p47phox and PCNA in a dose-dependent manner, with an equilibrium dissociation constant (K_D) value within the nanomolar range ($K_D = 7.7 \times 10^{-8}$ M; Fig. 1 A and Table 2). No direct interaction was detected between PCNA and p67phox or p40phox, whereas Rac2 could interact with PCNA with a micromolar-range affinity. To identify the domain of p47phox involved in PCNA interaction, we first examined if this interaction could be prevented by phosphoinositides that can bind to the PX domain (residues 1–141) that is crucial for p47phox membrane association (Kanai et al., 2001). When phosphoinositides and p47phox were preincubated before injection over immobilized PCNA, the percentage of p47phox binding to PCNA was decreased in a dose-dependent manner (Fig. 1 B). In keeping with this hypothesis, recombinant PX domain generated as a truncated p47phox protein showed a direct interaction with PCNA, although the calculated K_D was higher than that of full-length p47phox. This suggests that either p47phox binding is dependent on the conformation of the PX domain in intact p47phox or other p47phox domains are involved in PCNA binding (Fig. 1 C and Table 2).

Many PCNA-interacting proteins including p21/waf1 contain a conserved sequence known as PCNA-interacting protein box (PIP-box) with a consensus sequence of [Q]xx[h]XX[a][a], where h stands for hydrophobic and a for aromatic residues (Fig. S1). We identified four peptide sequences (p47phox-46-67, p47phox-63-90, p47phox-83-110, and p47phox-106-127) containing a PIP-box motif that were not buried in p47phox PX domain (Fig. 1 D) sequence. The corresponding p47phox peptides were tested for their binding capacity to PCNA by SPR and were compared with the p21-141-160-peptide used as a positive control ($K_D \approx 10^{-7}$ M) and to the mutant p21 peptide deprived of PCNA binding sites as a negative control (Zheleva et al., 2000; Warbrick, 2006). Peptides p47phox-46-67, p47phox-63-90, and p47phox-83-110 did not interact with PCNA, while p47phox-106-127 showed a direct interaction with PCNA (Fig. 1 E and Table 2). Interestingly, the p47phox-106–127 peptide and the p47phox PX domain bind PCNA with a similar affinity ($K_D \approx 5 \times 10^{-5}$ M; Table 2), strongly suggesting that the p47phox-106-127 sequence was mainly responsible for the p47phox PX–PCNA interaction.

Coinjection of p21 peptide (2, 5, or 8 µM) with the p47phox over immobilized PCNA decreased the binding of p47phox to PCNA in a dose-dependent manner, compared with binding in the absence of the p21 peptide (Fig. 1 F). Likewise, similarly to the p21 peptide and in agreement with its ability to bind PCNA, the p47phox-106-127 peptide inhibited the interaction between PCNA and the p47phox protein in a dose-dependent manner, as measured by SPR. These data unambiguously demonstrated that the interdomain-connecting loop of PCNA was involved in the interaction with p47phox and strongly suggested that this interaction was mediated by the p47phox PX domain mapping the 106–127 residues.

To further ascertain the molecular association between PCNA and p47phox-106-127 peptide, crystallization assays and diffraction analysis were used. Crystals could be grown under several different conditions, but one (see Materials and methods for details) provided reproducible crystals diffracting at ∼3-Å resolution. The unit cell dimensions and the crystal packing were similar for all crystals (Figs. 2 A and S1, B–D). However, the space group was found to be either orthorhombic ($P2_12_12_1$, one trimer in the asymmetric unit) or monoclinic ($P2_1$, two trimers in the asymmetric unit). Our attempts to cocrystallize intact p47phox or its PX domain together with PCNA were unsuccessful and were hampered by the flexible p47phox structure. However, we could obtain crystallographic data by soaking PCNA crystals in solutions containing 100–500 µM of p47phox-106-127 peptide for 24 h before data collection. Complete

Table 1. **Proteins involved in signaling and oxidant-related processes identified by MS in the material eluted from the anti-PCNA coimmunoprecipitation in neutrophil cytosol**

Swiss-Prot ID	Protein name	Molecular weight	Gene name	UniProt ID
Ubiquitin				
UBA1_HUMAN	Ubiquitin-like modifier-activating enzyme 1	117.8	UBA1	P22314
Cytoskeleton				
PROF1_HUMAN	Profilin-1	15.1	PFN1	P07737
FLNA_HUMAN	Filamin-A	280.7	FLNA	P21333
MOES_HUMAN	Moesin	67.8	MSN	P26038
VINC_HUMAN	Vinculin	123.8	VCL	P18206
ARC1B_HUMAN	Actin-related protein 2/3 complex subunit 1B	40.9	ARPC1B	O15143
Oxidant-related proteins				
PDIA1_HUMAN	Protein disulfide-isomerase	57.1	P4HB	P07237
THIO_HUMAN	Thioredoxin	11.7	TXN	P10599
GTP-binding protein				
IQGA1_HUMAN	Ras GTPase-activating-like protein IQGAP1	189.3	IQGAP1	P46940
GDIB_HUMAN	Rab GDP dissociation inhibitor β	50.7	GDI2	P50395
GDIR1_HUMAN	Rho GDP-dissociation inhibitor 1	23.2	ARHGDIA	P52565
GDIR2_HUMAN	Rho GDP-dissociation inhibitor 2	23	ARHGDIB	P52566
NADPH oxidase				
NCF1_HUMAN	Neutrophil cytosol factor 1; p47phox	44.8	NCF1	P14598
NCF2_HUMAN	Neutrophil cytosol factor 2; p67phox	59.8	NCF2	P19878
NCF4_HUMAN	Neutrophil cytosol factor 4; p40phox	39	NCF4	Q15080
COR1A_HUMAN	Coronin-1A	51	CORO1A	P31146
G-coupled protein				
GNAI2_HUMAN	Guanine nucleotide-binding protein G(i) subunit α-2	40.5	GNAI2	P04899
Glycolysis				
G3P_HUMAN	Glyceraldehyde-3-phosphate dehydrogenase	36.1	GAPDH	P04406
G6PD_HUMAN	Glucose-6-phosphate 1-dehydrogenase	59.3	G6PD	P11413
G6PI_HUMAN	Glucose-6-phosphate isomerase	63.1	GPI	P06744
6PGD_HUMAN	6-Phosphogluconate dehydrogenase	53.1	PGD	P52209
6PGL_HUMAN	6-Phosphogluconolactonase	27.5	PGLS	O95336
ALDOA_HUMAN	Fructose-bisphosphate aldolase A	39.4	ALDOA	P04075
ALDOC_HUMAN	Fructose-bisphosphate aldolase C	39.5	ALDOC	P09972
HXK1_HUMAN	Hexokinase-1	102.5	HK1	P19367
LDH6B_HUMAN	L-lactate dehydrogenase A-like 6B	41.9	LDHAL6B	Q9BYZ2
LDHA_HUMAN	L-lactate dehydrogenase A chain	36.7	LDHA	P00338
LDHB_HUMAN	L-lactate dehydrogenase B chain	36.6	LDHB	P07195
KPYM_HUMAN	Pyruvate kinase isozymes M1/M2	57.9	PKM	P14618

Immunoprecipitation of PCNA was performed in cytosols from human neutrophils obtained by nitrogen cavitation, and proteins associated with PCNA were identified by MS. This representative experiment was performed two times on two different cytosols with similar results.

crystallographic data were collected on ∼50 crystals, with a maximum resolution varying from 4.2 to 2.8 Å, and the PCNA structure was determined for all these crystals by molecular replacement using the PCNA 1AXC structure. In five crystals, we observed a significant positive electron density on the residual (F_{obs} – F_{calc}) electron density map, indicating that the p47phox-106-127 peptide could bind the PCNA interdomain-connecting loop region (Fig. 2 B).

Although the maximum resolution (3.22 Å) and the occupancy of the bound peptide obtained for these five crystals was

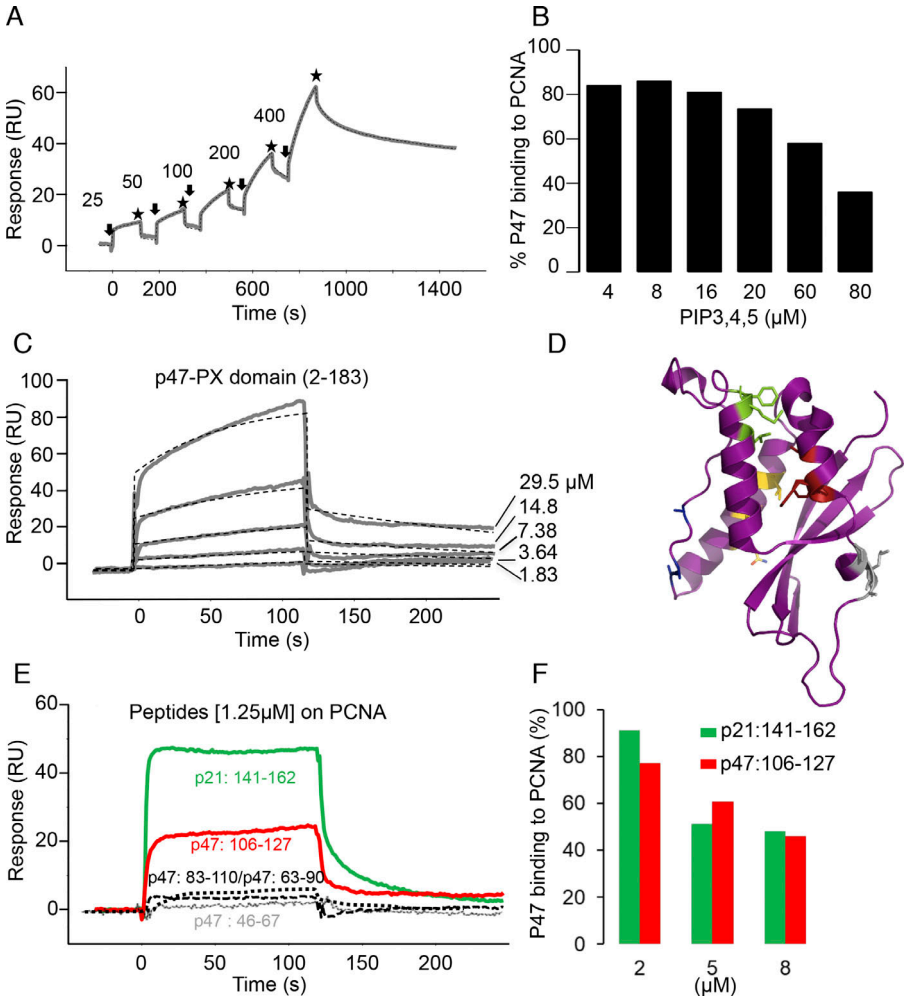


Figure 1. **Molecular investigation of the binding between p47phox and PCNA. (A)** SPR analysis of the interaction of p47phox (nanomoles) over immobilized PCNA. Arrows and stars indicate the injection start and end points for each p47phox concentration. Fit obtained with a statistic χ^2 value 0.24 is shown as dotted line (response units). **(B)** The phosphoinositide PIP3,4,5 inhibits p47phox–PCNA interaction. P47phox was incubated with PIP3,4,5 at various concentrations before injection on PCNA. Binding was expressed as percentage of p47phox binding measured without PIP3,4,5. **(C)** SPR measurements of p47phox PX domain interaction on PCNA. Data represent overlays of sensograms resulting from injection of p47phox-PX domain at different concentrations (micromoles). Fits with a statistic χ^2 value 1.5 are shown as dotted lines (response units). **(D)** Putative PIP-box localization within the p47phox PX domain, shown in purple. PIP-boxes 46–67, 63–90, 83–110, and 106–127 are depicted in green, blue, yellow, and red, respectively. The helix turn structurally similar to p21 PIP-box is depicted in silver. **(E)** Comparative binding of p21, p47phox-46-67, p47phox-63-90, p47phox-83-110, and p47phox-106-127 peptides on PCNA. **(F)** P21 peptide and p47phox-106-127 interfere with p47phox–PCNA association measured by SPR. The p21 peptides and p47phox-106-127 at various concentrations were coinjected with p47phox over PCNA as in B. Results are expressed as the percentage of p47phox binding measured without competing peptide. SPR experiments were performed three times with identical results on either a Biacore 3000 (C–E) or a Biacore T200 (A and B) apparatus. Kinetic values determinations for p47/PCNA and p47-PX domain/PCNA interactions are reported in Table 2.

too low to determine unambiguously the amino acids of p47phox-106-127 involved in the interaction with PCNA, we propose two computational models of the complex between PCNA and p47phox PX domain, based on structures available in the Protein Data Bank (PDB). We used the structure of the complex between the p21 peptide (mapping the 141–160 residues) and PCNA (PDB entry 1AXC; Gulbis et al., 1996) and the structure of the p47phox PX domain (PDB entry 1KQ6). In the first option, structural analysis of the 1KQ6 structure showed that the 114–118 PIP-box of p47phox was partially buried and should adopt another conformation to be able to interact with PCNA. Therefore, the p47phox PX-106-127 region has been modeled to adopt a conformation close to the one adopted by p21 in 1AXC structure (Fig. 2 C). If such a mode of interaction is plausible, as it generates no steric hindrance, it relies on a hypothetical conformational change in the 106–127 region of the p47phox PX domain that remains to be experimentally observed. The second option was to search for regions of the p47phox PX that adopt a conformation that is similar to the one adopted by the p21 peptide, when bound to PCNA. The 122–126 region of the p47phox PX domain is structurally very similar to the 147–151 region of p21 (root mean square difference of 0.25 Å) and corresponds to the core of the PIP-box that was structurally conserved in numerous PCNA-peptide complex structures. By superimposing the 122–126 residues of 1KQ6 p47phox PX structure on the 147–151 region of 1AXC PCNA/p21 peptide, we built a plausible PCNA-p47phox PX domain complex with no steric clashes (Fig. 2 D). The distinction between these two possibilities should await the crystal structure of p47phox protein, which is not yet publicly available.

PCNA is involved in NOX2 activation in intact cells

To address the functional impact of the PCNA–NOX2 interaction, we first used neutrophil-like differentiated PLB985 cells, an established model of human neutrophils, which allow transfection experiments. We previously reported that in proliferating nondifferentiated PLB985 cells, PCNA is nuclear (Fig. 3 A) but becomes exclusively cytosolic after differentiation, therefore representing a suitable surrogate for human neutrophils (De Chiara et al., 2013). Differentiated PLB985 cells that stably overexpress PCNA as previously described (Witko-Sarsat et al., 2010) showed a marked increase in PMA- and opsonized zymosan (OZ)–induced superoxide production compared with PLB985 cells stably transfected with control plasmid (Fig. 3, B

Table 2. **Kinetics and affinity of PCNA interaction with cytosolic components of NADPH-oxidase**

Immobilized ligand/soluble analyte	PCNA				
	k_{a1} ($M^{-1}s^{-1}$)	k_{d1} (s^{-1})	$k_{forward}$ (s^{-1})	$k_{backward}$ (s^{-1})	K_D (M)
p47phox (two-state model)	8.7×10^3	8.4×10^{-3}	7.5×10^{-3}	6.5×10^{-4}	7.7×10^{-8}
p47-PX domain (1:1 model)	85.2	2.8×10^{-3}	NA	NA	3.3×10^{-5}
p47 peptide 106–127	1.0×10^4	0.35	NA	NA	3.4×10^{-5} (K_{D1})
(Heterogeneous ligand model)	160	0.0111	NA	NA	6.9×10^{-5} (K_{D2})
p47 peptides					
83–110	ND	ND	ND	ND	ND
63–90					
46–67					
Rac2 (two-state model)	541	17×10^{-3}	5.7×10^{-3}	6.6×10^{-4}	3.3×10^{-6}

No significant binding was detected for p40phox and p67phox for concentrations ≤1 µM. The binding of PCNA with p47phox (25–400 nM), p47-PX domain (1.83–29.5 µM), or p47peptide 106–127 (0.31–40 µM) was investigated by SPR as described in Materials and methods. Kinetics parameters were calculated using either two-state, 1:1 Langmuir, or heterogeneous ligand reactions models. For the two-state binding model ($A + B \leftrightarrow AB \leftrightarrow AB^*$) that fit the best for full-length p47phox, k_{a1}, k_{d1}, $k_{forward}$, and $k_{backward}$ constants were determined by global fitting. The dissociation constant K_D was determined from the $(k_{d1}/k_{a1})/(1 + k_{forward}/k_{backward})$ ratio. The heterogeneous ligand model accounts for two different binding sites on the immobilized PCNA, and the corresponding two kinetic values were calculated. For 1:1 Langmuir and heterogeneous ligand models, the equilibrium dissociation constant is calculated by $K_D = k_d/k_a$. The data presented were obtained with a statistic χ^2 value <2. Rac2, p40phox, and p67phox were also tested for their interaction with PCNA. Binding of Rac2 (0.51–8, 2 µM) to PCNA was measured and evaluated as reported below (χ^2 value 0.6). NA, not applicable; ND, the very low binding signal detected for p47 83–110, 63–90, and 46–67 peptides did not allow evaluation of kinetic data.

and C). Increased PMA-induced ROS production in PCNA-overexpressing cells was confirmed by 2′,7′-dichlorofluorescin diacetate (DCF-DA) FACS analysis. Notably, this increase in PMA-induced ROS production was abolished when PLB985 cells were transfected with PCNA fused to the SV40 nuclear localization sequence (NLS), thereby excluding from the cytosol (Bouayad et al., 2012; Fig. 3, D and E). Transfection of PCNA siRNA efficiently down-regulated PCNA protein expression (Fig. 3 F) and significantly decreased ROS production measured by luminol chemiluminescence (CL) in response to PMA and OZ (Fig. 3, G and H). Likewise, we used dimethylformamide (DMF)-differentiated PLB985 cells overexpressing the protein p21/waf1 (Fig. 3 I), which can bind PCNA and inhibit its antiapoptotic function (Martin et al., 2016). DMF-differentiated PLB985-p21A45R cells have significantly decreased NADPH oxidase activity triggered by either PMA or OZ relative to the PLB985 cells expressing an empty plasmid (Fig. 3, J and K). Notably, the effect of inhibiting PCNA on NADPH oxidase function is not merely a consequence of loss of neutrophil viability. The decreased NADPH oxidase function in differentiated PLB985 cells by PCNA inhibition (by either siRNA or ectopic expression of p21/waf1) was evident at time points in the absence of significant cell death (Fig. S2, A and B). Altogether, these results demonstrated that cytosolic PCNA controlled NADPH oxidase–dependent ROS production in intact cells.

Inhibition of PCNA–p47phox interaction hindered NADPH oxidase activation

We next examined if targeting PCNA could affect NADPH oxidase assembly in a cell-free system consisting of the cytosolic fraction containing PCNA and the NADPH oxidase components (p47phox, p67phox, p40phox, rac2) and the membrane fraction containing gp91phox and p22phox isolated from resting human neutrophils. NADPH oxidase activation was triggered by Li-SDS and the production of superoxide anions was measured by the cytochrome c reduction assay. The specificity of this assay was validated by the inhibitory effect of superoxide dismutase (SOD) or diphenylene iodonium (DPI), a NADPH oxidase inhibitor (Fig. 4 A). In this cell-free system, we tested the effect of the p21 peptide (Fig. 4 B) and T2 amino alcohol (T2AA), a nonpeptide cell-permeable PCNA inhibitor (Punchihewa et al., 2012; Inoue et al., 2014). Both compounds bind specifically to the PCNA interdomain-connecting loop to inhibit interactions with its partners (Fig. 4 C). Each compound led to a dose-dependent decrease in superoxide anion production, thereby demonstrating that PCNA was involved in NOX2 activation. T2AA also decreased PMA-, formyl-methionyl-leucyl phenylalanine (f-MLF)–, and OZ-induced NADPH oxidase activation in intact neutrophils measured by luminol CL in a dose-dependent manner (Fig. 4, D–F). The inhibitory effect of T2AA on ROS production was not related to apoptosis induction, since no Annexin-V labeling was detected on neutrophils after 1-h T2AA treatment up to a concentration of 50 µM in the presence of PMA (Fig. S2, C and D). Moreover, inhibition of caspases by the pan-caspase inhibitor Z-VAD(OMe)-FMK (Z-VAD) did not abrogate the inhibitory effect of T2AA on f-MLF–induced respiratory burst (Fig. S2, E and F). To further characterize the interaction between PCNA and p47phox, we examined whether PCNA, like cytosolic NADPH oxidase components, could translocate to the membrane upon PMA activation. Western blot analysis of neutrophil membranes and cytosol clearly showed that both p47phox and PCNA translocated to the membrane fraction upon PMA activation

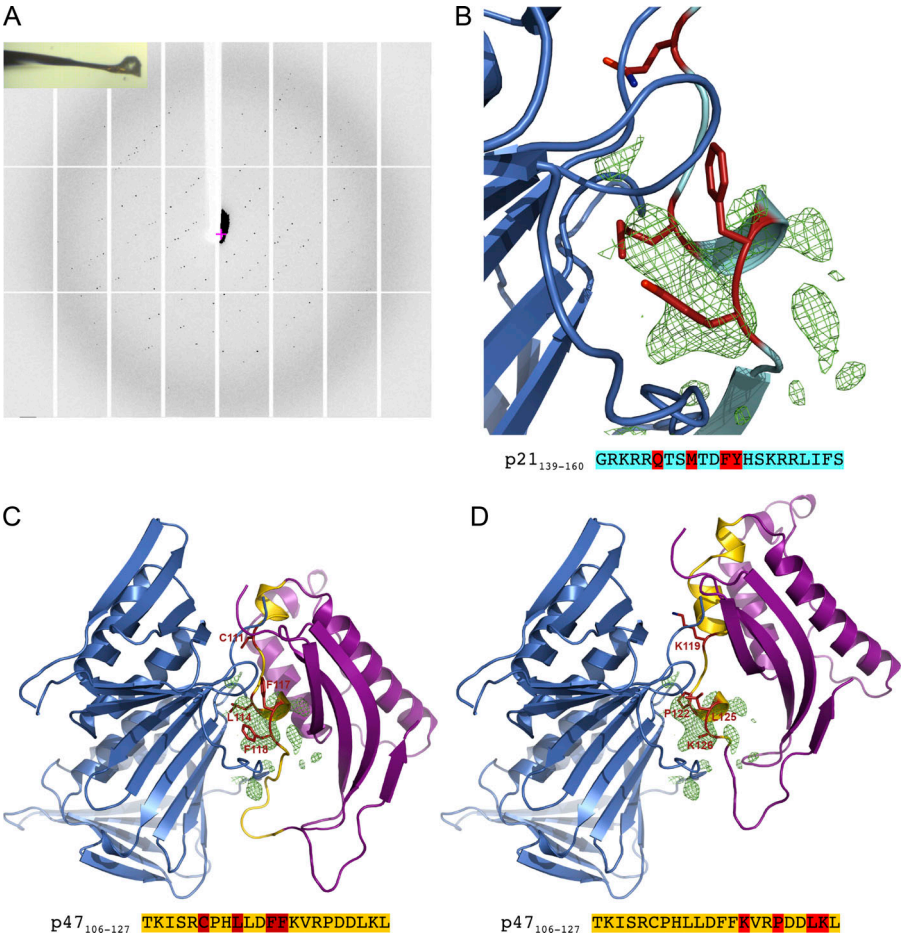


Figure 2. **Electron density map of PCNA crystals associated with the p47phox-106-127 peptide and molecular modeling of the complex PCNA-p47phox PX domain. (A)** Diffraction pattern of PCNA crystals soaked in p47phox-106-127 peptide solution and snapshot of the frozen crystal. This experiment was performed three times with identical results. **(B)** Residual (F_{obs} – F_{calc}) electron density map from 3.23-Å-resolution crystallographic data. The three highest peaks of the residual (F_{obs} – F_{calc}) electron density map (green) are located where PIP-box–containing peptides interact with PCNA. The p21-139-160 peptide from PCNA-p21-139-160 peptide complex structure (PDB entry 1AXC) in cyan with the four main residues of the PIP-box highlighted in red. **(C and D)** Two putative models of PCNA-p47phox-PX domain complex based on the crystal structures of human PCNA (blue) the structure of p21-139-160 peptide (cyan) bound to PCNA and the p47phox PX domain (purple) with the residues 106–127 (gold). Predicted PIP-box residues are depicted in red. **(C)** Model based on the putative PIP-box of the p47phox-106-127 peptide whose conformation has been modified to fit the p21 peptide structure. **(D)** Model based on the structural homology between the helix turn of p47phox-122-126 and of the p21-PIP-box.

(Fig. 4 G). Notably, T2AA inhibited p47phox translocation to the membrane during activation without inhibiting its phosphorylation. Consistent with a direct interaction between p47phox and PCNA, we observed that PCNA and p47phox colocalized in cytosol in unstimulated neutrophils by confocal microscopy analysis after indirect immunofluorescence labeling (Fig. 5 A). Using Duolink technology, a proximity ligation assay, we provided evidence that PCNA and p47phox are in close proximity within the cytosol of resting neutrophils (Fig. 5 B). In contrast, p47phox and rac2, two cytosolic proteins known to localize in separate cytosolic complexes in resting neutrophils, did not demonstrate proximity, supporting the specificity of this technology. Interestingly, PCNA and p47phox proximity was strongly decreased after PMA activation. Notably, immunoprecipitation of PCNA in the cytosol of resting neutrophils showed that it coimmunoprecipitated with p47phox (Fig. 5 C). However, the amount of p47phox associated with PCNA was strongly decreased after PMA or f-MLF stimulation. Taken together, our results suggested that PCNA associates with p47phox in cytosol of resting neutrophils and facilitates NADPH oxidase assembly. The association is disrupted after activation, although PCNA could translocate to the plasma membrane. Importantly, T2AA did not inhibit other antipathogen functions such as f-MLF–induced degranulation, C5a- or f-MLF–induced chemotaxis, and *Escherichia coli* phagocytosis tested in vitro on isolated neutrophils (Fig. S3).

Destabilization of PCNA scaffold by T2AA inhibits NADPH oxidase activity in vivo

We next evaluated whether inhibiting the interaction between PCNA and p47phox using T2AA would inhibit NADPH oxidase activity in vivo in inflammatory neutrophils during zymosan-induced peritonitis in mice (Martin et al., 2016). Peritoneal lavages were collected 4 h after zymosan injection, and inflammatory cells including neutrophils and macrophages were analyzed by FACS. T2AA did not have any significant effect on the total number of cells (Fig. 6 A) or the cellular composition in the lavage fluid (Fig. 6, B and C). Peritoneal neutrophils from T2AA-treated mice showed decreased ex vivo ROS production compared with controls (Fig. 6 D), thereby confirming our in vitro results on human neutrophils (Fig. 4 D). We next used in vivo noninvasive imaging of neutrophil activation using L012-enhanced CL (Kielland et al., 2009) to demonstrate that T2AA could inhibit NADPH oxidase in situ. Zymosan-induced peritonitis increased L012-CL in the peritoneum, and T2AA significantly attenuated this (Fig. 6, E and F). In our previous study, we had shown that p21/wafl protein acts as a specific inhibitor of the PCNA scaffold in inflammatory neutrophils (Martin et al., 2016). We further investigated NADPH oxidase activation in inflammatory neutrophils in p21/wafl$^{-/-}$ mice. PMA-induced ROS production was significantly increased in peritoneal lavage neutrophils from p21/wafl$^{-/-}$ mice compared with neutrophils from WT mice, confirming that binding of p21/wafl to PCNA restrains NADPH oxidase activation (Fig. 6, G and H).

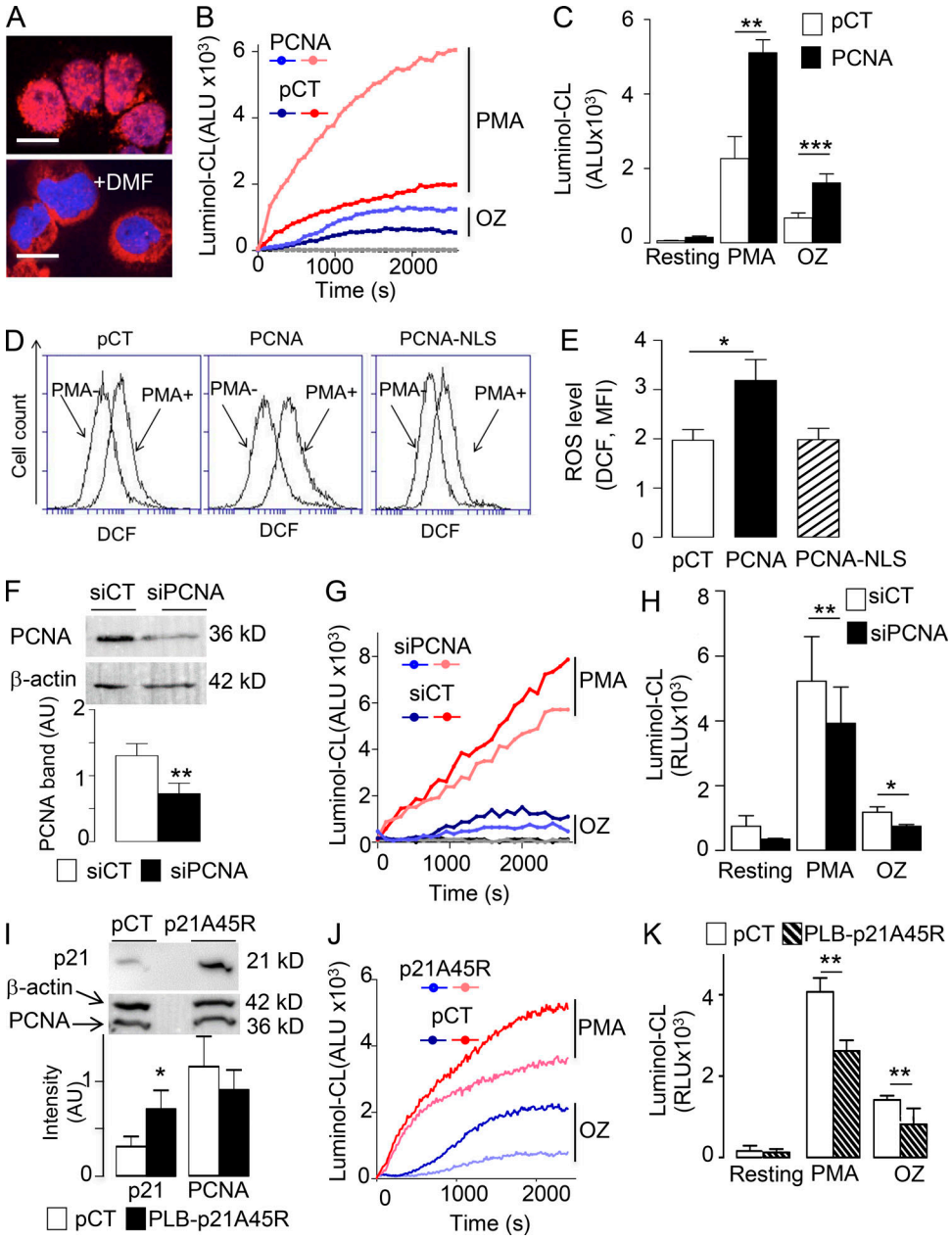


Figure 3. **PCNA controls ROS production in differentiated PLB985 cells. (A)** Representative experiment out of 10 showing the detection of cytosolic PCNA by immunofluorescence in DMF-differentiated PLB985 cells. The scale bars correspond to 10 µm, magnification 63×. **(B)** Kinetic analysis of luminol-CL in DMF-differentiated PLB985 cells transfected with a control (pCT) or with a PCNA-coding plasmid stimulated or not (resting) with PMA or OZ. **(C)** CL peaks corresponding to B were expressed as mean ± SEM of four independent experiments performed in duplicate. **(D)** FACS plots of DCF-mediated fluorescence in PLB985-overexpressing PCNA or a nuclear form of PCNA (PCNA-NLS) versus control (pCT). Representative experiment before (–) and after (+) PMA out of four sets of independent experiments. **(E)** Quantification of DCF-MFI. Data are mean ± SEM (n = 10 for PCNA WT and CT, n = 4 for PCNA NLS). **(F–H)** Effect of PCNA siRNA on NADPH oxidase activation. **(F)** Western blot analysis of PCNA and actin expression after siRNA-PCNA treatment compared with siRNA-CT (upper panels) and quantification of PCNA/β-actin ratio expressed as mean ± SEM of four independent experiments performed in duplicate (lower panel). **, $P < 0.01$, Mann–Whitney U test. **(G)** Kinetic analysis of luminol-CL of DMF-differentiated PLB985 cells stimulated with PMA or OZ compared with resting. **(H)** CL peaks corresponding to G expressed as mean ± SEM of four independent experiments performed in duplicate. **(I–K)** Effect of p21/Waf1 expression on NADPH oxidase activation. **(I)** Western blot analysis of p21/waf1, PCNA, and actin expression (upper panel) and quantification of PCNA/β-actin ratio expressed as mean ± SEM of three independent experiments performed in duplicate (lower panel). *, $P < 0.01$, Mann–Whitney U test. **(J)** Kinetic analysis of luminol-CL of DMF-differentiated PLB985 cells transfected with a p21/waf1-coding plasmid or a control plasmid (pCT) and stimulated with PMA or OZ. **(K)** CL peaks corresponding to J expressed as mean ± SEM of eight independent experiments performed in duplicate. ANOVA test was performed (C, E, H, and K): *, $P < 0.05$; **, $P < 0.01$; ***, $P < 0.001$.

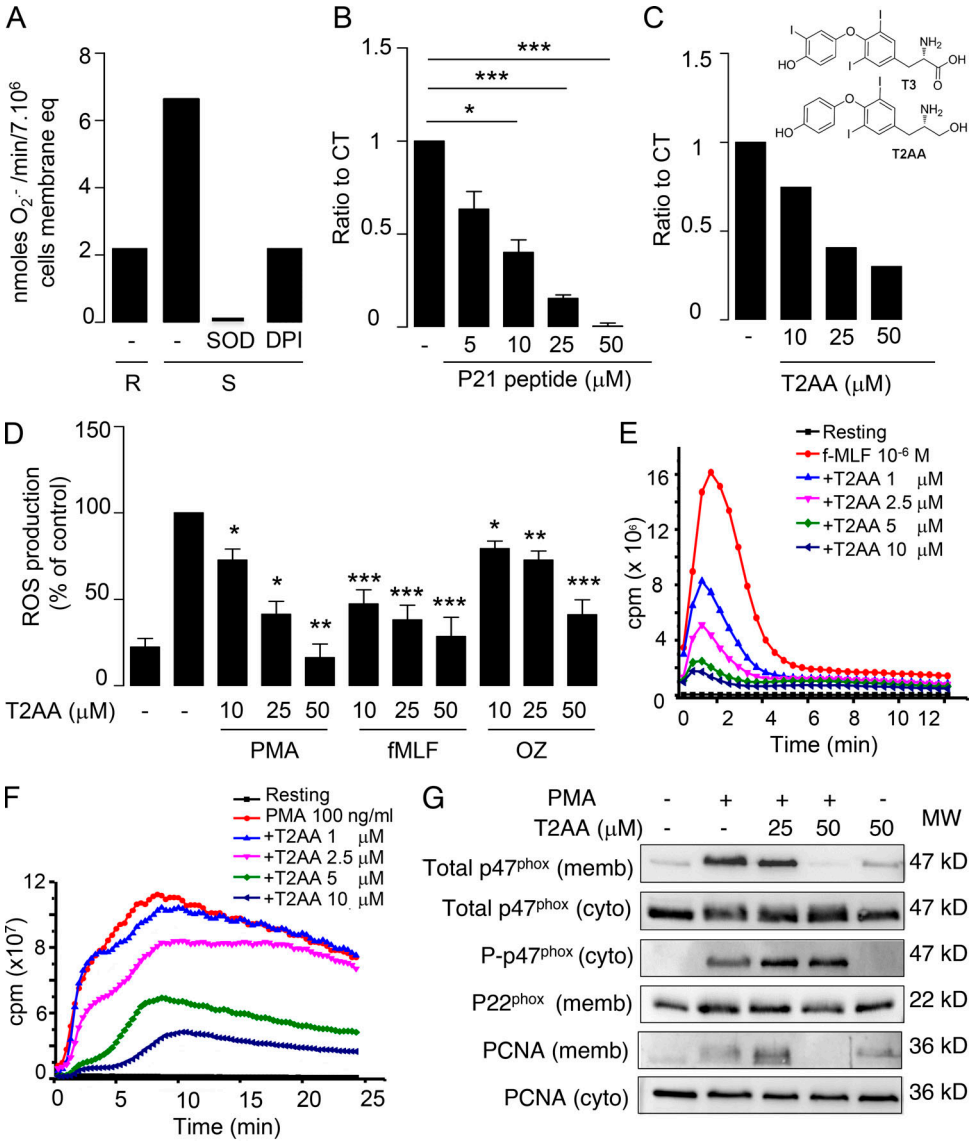


Figure 4. **Inhibition of NADPH oxidase activation by targeting the interdomain-connecting loop of PCNA. (A–C)** Effect of PCNA inhibitors on NADPH oxidase activation in a cell-free system. **(A)** Typical experiment representative of three independent experiments performed in different blood donors showing superoxide anion production by cytosols and membranes purified from human neutrophils and stimulated by the addition of Li-SDS (S). No superoxide anion was observed in resting (R) or in the presence of SOD or DPI. Results are expressed as nanomoles of $O_2^{\cdot-}$/min/7 × 10^6 cell membrane equivalent. **(B and C)** Effect of p21-peptide (B) or T2AA (C) on superoxide anion production in the cell-free system described in A. Results are ratio of superoxide anion production to untreated positive control. Data are mean ± SEM for p21-peptide (n = 3; *, P < 0.05, paired Student's t test) and for T2AA (n = 2). **(D)** Inhibitory effect of T2AA on NADPH oxidase activation in neutrophils stimulated with PMA (n = 4), f-MLF (n = 7), or OZ (n = 10). NADPH oxidase activation was evaluated by luminol-CL expressed as ratio to the untreated stimulated cells. The data are mean ± SEM of the indicated number of independent experiments performed in duplicate (*, P < 0.05; **, P < 0.01; ***, P < 0.001, ANOVA). **(E and F)** Representative kinetic analysis of luminol-CL in neutrophils stimulated with f-MLF (E) or PMA (F) compared with resting in the presence or absence of T2AA (1–10 μM). **(G)** Effect of T2AA on membrane translocation of PCNA and p47phox. Neutrophils pretreated with or without T2AA for 1 h were stimulated with PMA. Proteins (PCNA, p47phox, phospho-p47phox, and p22phox) contained in the membrane (memb) or the cytosolic (cyto) fractions were analyzed by Western blot. This experiment is representative of three independent experiments performed in different blood donors yielding the same results.

As we previously reported that PCNA inhibition by the p21 peptide promotes neutrophil apoptosis, we examined whether T2AA could also affect neutrophil survival. Indeed, T2AA did not induce ex vivo apoptosis in resting bone marrow neutrophils but induced dose-dependent apoptosis in inflammatory neutrophils isolated from peritoneal lavages (Fig. S4 A). Analysis of neutrophils from WT and p47phox$^{-/-}$ mice (Kasahara et al., 1997) showed that this proapoptotic effect of T2AA on inflammatory neutrophils was not dependent on the presence of p47phox (Fig. S4 B). From this set of data, we conclude that T2AA triggered apoptosis preferentially in neutrophils at the inflammatory site without affecting their survival in bone marrow.

T2AA exerts a potent antiinflammatory effect in TNBS-induced colitis

As T2AA inhibited ROS production in inflammatory neutrophils, we investigated whether it could exert an antiinflammatory effect in TNBS-induced colitis (Wallace et al., 1989), as this

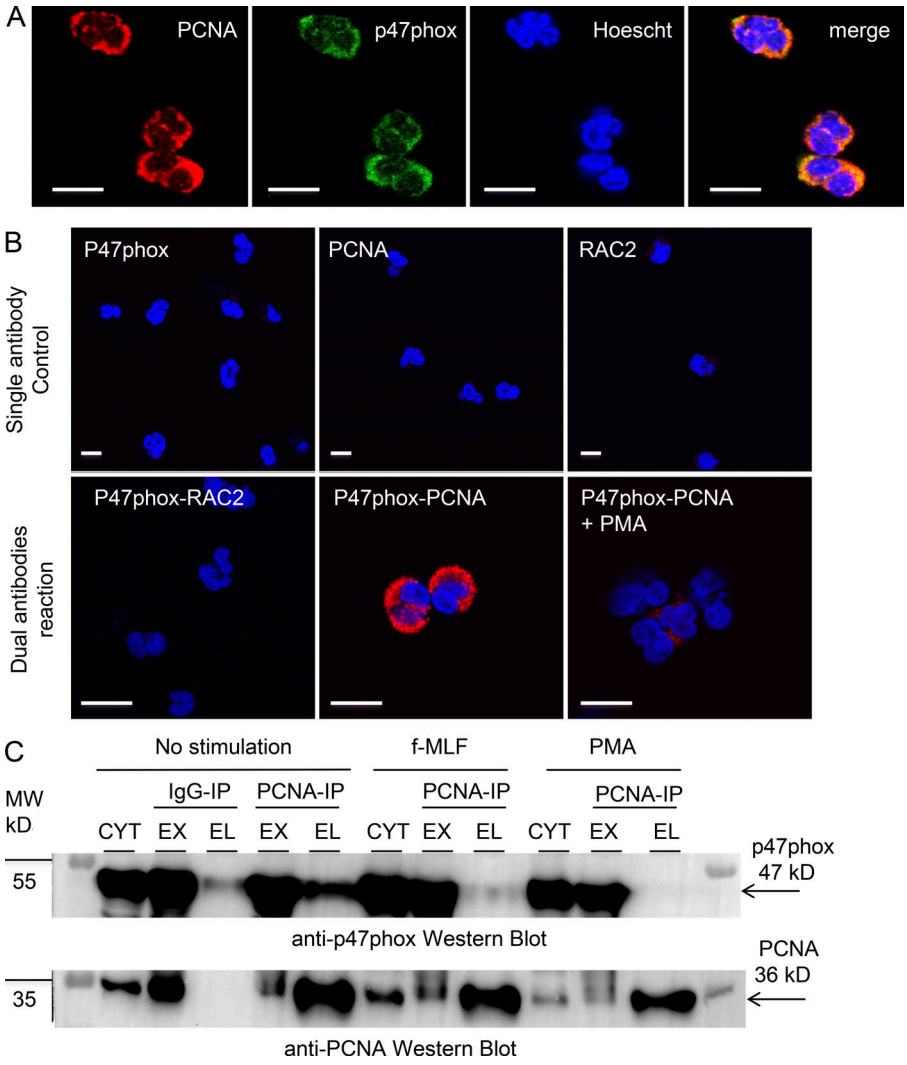


Figure 5. **Colocalization and coimmunoprecipitation of PCNA and p47phox in human neutrophils. (A)** Colocalization of PCNA and p47phox shown by indirect immunofluorescence using a polyclonal rabbit anti-PCNA and a mAb anti-p47phox, respectively. **(B)** Colocalization of PCNA and p47phox using the Duolink technology. The upper panels show negative controls using a single antibody. The lower panels show the fluorescence in the presence of two antibodies: p47phox and rac2; p47phox and PCNA in the absence or in the presence of PMA. Hoechst was used for nuclear staining. A and B show representative experiments of three yielding the same results. Fluorescence was analyzed by confocal microscopy. In A and B, the scale bars correspond to 10 µm, magnification 63×. **(C)** Western blot analysis of coimmunoprecipitation between PCNA and p47phox in cytosol (CYT) of neutrophils without stimulation or after activation with f-MLF or PMA. Unbound material in the exclusion fraction (EX) and bound immunoprecipitated proteins recovered in the elution fraction (EL) were analyzed by Western blot analysis as described in Materials and methods. This experiment is representative of three independent experiments performed in different blood donors yielding the same results. MW, molecular weight.

model is dependent on early massive recruitment of neutrophils (Krimi et al., 2008). Mice received two doses of T2AA or vehicle by intraperitoneal injection after TNBS treatment. The increase in colonic weight/length ratio induced by TNBS, a macroscopic indicator of inflammation, was significantly decreased in the presence of T2AA (Fig. 7 A). These data were supported by the lower Wallace score in T2AA-treated mice, reflecting less extensive inflammatory lesions, with a mean percentage of protection of 50.9 ± 8.8% (Fig. 7 B). Histological analysis confirmed that TNBS induced strong acute colonic inflammation and necrosis, with extensive ulceration in untreated animals (Fig. 7 D). The colons of T2AA-treated mice displayed less ulceration and more advanced healing of the eroded surface. Reepithelization and regeneration of colonic mucosa were illustrated respectively by colonization of the ulcer surface by epithelial cells and by mucosal repair of neighboring ulceration with gland hyperplasia and numerous mitotic cells. The T2AA beneficial effect was demonstrated by reduction in the Ameho score (Ameho et al., 1997), reflecting less-severe histological tissue damage (Fig. 7 C). To evaluate tissue oxidative stress, we assessed the presence of myeloperoxidase (MPO), the enzyme responsible for the generation of chlorinated oxidants by active neutrophils in the colon. Notably, MPO immunohistochemical staining was strongly decreased in the colonic epithelium of T2AA-TNBS–versus TNBS-treated mice, demonstrating a reduced number of neutrophils present in T2AA-TNBS colon (Fig. 7 D). We also evaluated in vivo ROS-mediated tissue damage by measuring malondialdehyde (MDA), a product of lipid peroxidation, in colon homogenates (Fig. 7 E). Our results show a significant decrease in MDA concentrations in tissues from T2AA-treated mice compared with untreated mice, in agreement with decreased MPO content. Using the in vivo L012-based imaging method, we confirmed that neutrophil NADPH oxidase was activated in TNBS-induced colitis and that T2AA significantly decreased L012-CL, indicative of a neutrophil-targeted antiinflammatory effect (Fig. 7, F and G). Finally, neutrophil depletion was used to further ascertain that T2AA targeted activated inflammatory neutrophils. Neutrophil depletion using anti-Ly6G mAb (Coffelt et al., 2015; Fig. 8 A) resulted in a drastic loss of neutrophils in both blood and bone marrow compared with control IgG-treated mice (Fig. 8 B). Neutrophil depletion induced a significant decreased severity of colitis in the absence of T2AA as evidenced by the macroscopic analysis quantified by the Wallace score (Fig. 8 C). Notably, while T2AA exerted a

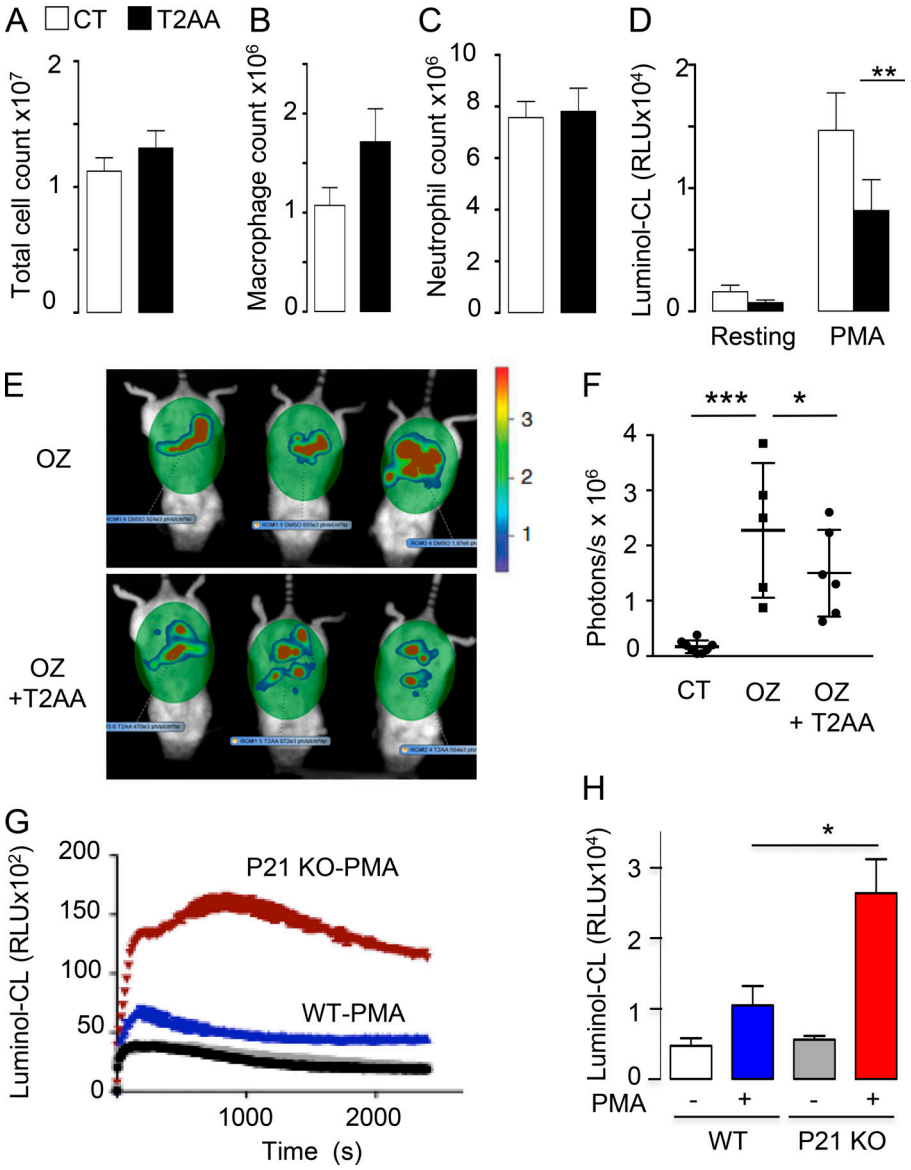


Figure 6. **Destabilization of PCNA scaffold inhibits NADPH oxidase activity in vivo. (A–C)** FACS analysis of cells in the peritoneal lavage 4 h after zymosan injection in mice treated with or without T2AA. Two independent sets of experiments were performed with a total of eight mice per group. **(A)** Total cell count. **(B)** Number of macrophages ($F4/80^+$). **(C)** Number of neutrophils ($Ly6G^+$). **(D)** Effect of T2AA on ex vivo neutrophil NADPH oxidase activity measured by luminol-CL in peritoneal neutrophils stimulated or not with PMA. The data are CL peaks expressed as mean ± SEM (n = 8). **, $P < 0.01$, ANOVA. **(E and F)** Inhibitory effect of T2AA on in vivo ROS production evaluated by L012-CL during zymosan-induced peritonitis. **(E)** Representative imaging of ROS production in individual mice. The pseudocolor heat maps represent photons/s/cm²/steradian. **(F)** Quantification of in vivo L012-CL in mice. The data are CL peaks expressed as mean ± SEM from five to six mice per group in two independent experiments; *, $P < 0.05$; ***, $P < 0.001$, ANOVA. **(G and H)** Ex vivo neutrophil NADPH oxidase activity measured by luminol-CL in neutrophils from WT or $p21^{-/-}$ mice isolated from the peritoneal lavage 4 h after zymosan injection stimulated or not with PMA (as in D). **(G)** Representative kinetic analysis of NADPH oxidase activation in neutrophils from WT compared with $p21^{-/-}$ mice. **(H)** The data are CL peaks expressed as mean ± SEM (from six mice per group in two independent experiments; *, $P < 0.05$, ANOVA).

significant antiinflammatory effect in IgG-treated mice, no effect of T2AA was observed in anti-Ly6G–treated mice. Histological evaluation and immunolabeling of neutrophils confirmed the strong decrease in neutrophils in the colon of anti-Ly6G–depleted and TNBS-treated mice (Fig. 8 E). Importantly, no beneficial effect of T2AA on colon inflammation assessed by neutrophil immunolabeling was observed in neutrophil-depleted mice, albeit with a lower baseline level of disease activity (Fig. 8 E). These new data show that the acute inflammation observed in TNBS-induced colitis as well as the antiinflammatory effect of T2AA are both dependent on the presence of neutrophils.

Discussion

To effectively limit neutrophil-mediated tissue inflammation and damage, therapeutic strategies should ideally target neutrophil release of toxic mediators such as excessive ROS while promoting neutrophil apoptosis and subsequent clearance. Therapies should avoid excessive impairment of neutrophil bone marrow production to limit immunosuppressive consequences. In the current study, we have uncovered a new role of cytosolic PCNA in the regulation of NADPH oxidase activity and highlighted the therapeutic potential of targeting PCNA.

The spatial separation of the NADPH oxidase components between cytosol and membrane and their interaction in complexes ensures that the enzyme is dormant in resting cells (Boussetta et al., 2010). In this setting, PCNA binds to the p47phox within the cytosol to restrain NADPH oxidase assembly and activation. Conversely, upon stimulation, PCNA bound to p47phox translocates to the membrane to facilitate NADPH assembly. Inhibiting PCNA prevents translocation without interfering with p47phox phosphorylation, thereby acting as a novel and unexpected regulator of neutrophil activation. It is noteworthy that, while almost all p67phox and p40phox are in a complex together with p47phox, excess p47phox can be found free of the other cytosolic proteins (Iyer et al., 1994; Park et al., 1994). This unbound p47phox has been shown to interact with

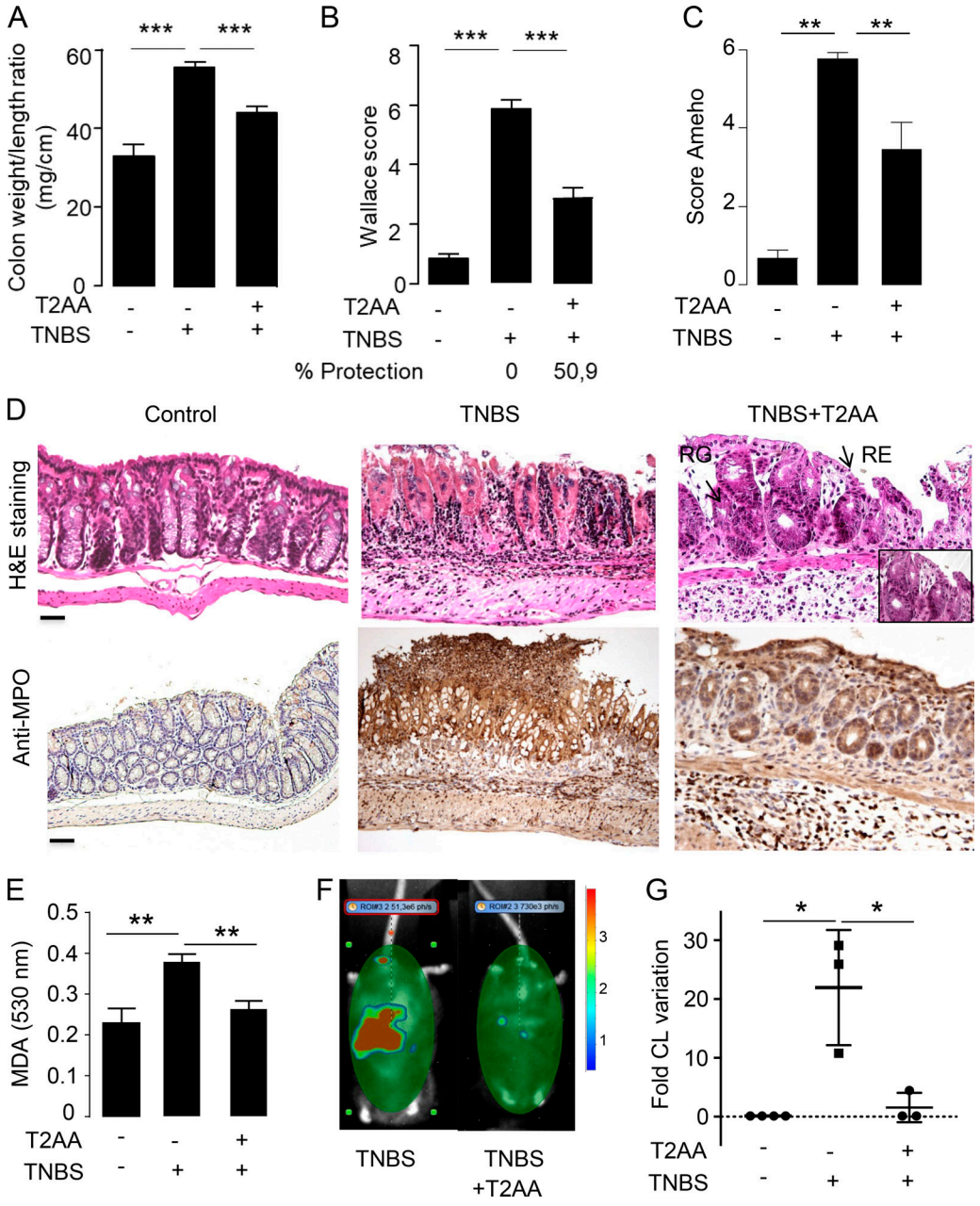


Figure 7. **Antiinflammatory effect of T2AA on TNBS-induced colitis. (A and B)** Macroscopic changes following TNBS treatment are represented by colon weight/length ratio (A) and Wallace score (B) in the respective histograms. **(C)** Ameho score representative of histological lesions is shown in the histogram. The data (A–C) are mean ± SEM (**, P < 0.01; ***, P < 0.001, ANOVA) from six to eight mice per group in two independent experiments. **(D)** Photomicrographs are representative of H&E-stained slides (upper panels) and of MPO immunohistochemical labeling (lower panels) of paraffin-embedded colonic tissues recovered from controls, TNBS alone, and TNBS and T2AA. The scale bars correspond to 20 µm, magnification 200×. RG, regeneration; RE, reepithelization. **(E)** Colorimetric measurement of MDA in colon. The data are mean ± SEM (n = 6); **, P < 0.01, ANOVA. **(F and G)** Inhibitory effect of T2AA on in vivo ROS production measured by L012-CL in TNBS-induced colitis mice. **(F)** Representative imaging of ROS production in individual mice with untreated TNBS-induced colitis (right panel) or T2AA-treated TNBS-induced colitis (left panel). This representative experiment shows the pseudocolor heat map representing photons/s/cm^2/steradian. **(G)** Quantification of in vivo L012-CL from three to four mice per group using the percentages of L012-CL variation between 24 and 48 h. The data are expressed as mean ± SEM (*, P < 0.05, nonparametric Wilcoxon test).

other cytosolic proteins including protein kinase C (Reeves et al., 1999) and phospholipase A2 (Shmelzer et al., 2008) and may be associated with PCNA. Other proteins identified as PCNA partners include cytoskeletal proteins, suggesting that this complex can facilitate the assembly of active NADPH oxidase complex at the membrane. Moreover, PCNA association with glycolysis enzymes, as previously shown in leukemic cells resistant to chemotherapy (Ohayon et al., 2016), strongly suggests that PCNA could be a link between survival, ROS production, and metabolism (Baillet et al., 2017).

We further demonstrated that PCNA binds to the PX domain of p47phox, in particular the region mapping the 106–127 residues

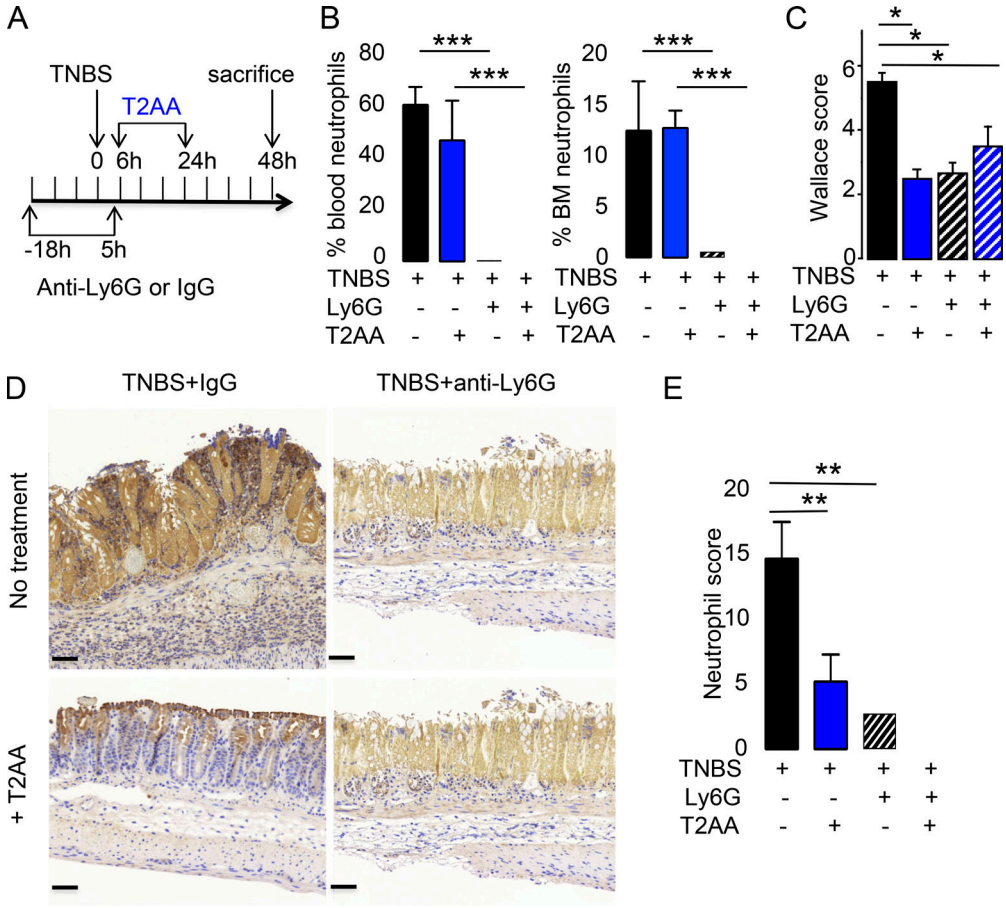


Figure 8. **Absence of T2AA antiinflammatory effect in TNBS-induced colitis following neutrophil depletion. (A)** Experimental protocol of colitis after neutrophil depletion using anti-Ly6G mAb. **(B and C)** Flow cytometry quantification of neutrophils in blood (left panel) and in bone marrow (right panel) in control (IgG) and neutrophil-depleted (Ly6G) mice. **(C)** Macroscopic changes following TNBS treatment measured by Wallace score. The data are mean ± SEM (ANOVA). **(D)** Representative photomicrographs of neutrophil immunostaining of colonic tissues with the neutrophil marker recovered from control (IgG) and neutrophil-depleted mice (Ly6G) treated with TNBS alone or TNBS combined with T2AA. The scale bars correspond to 20 µm, magnification 200×. **(E)** Quantification of neutrophil immunostaining as described in Materials and methods. In B, C, and E, the data are mean ± SEM. Two independent sets of experiments were performed with a total of eight mice per group. *, P < 0.05; **, P < 0.01; ***, P < 0.001, ANOVA.

involved in lipid binding. This is consistent with the notion that PCNA inhibits p47phox binding to the membrane in the resting state. Indeed the crystal structure of the isolated PX domain simultaneously bound to phosphatidylinositol 3,4-bisphosphate and phosphatidic acid revealed that the two lipids bind to two basic pockets (Karathanassis et al., 2002; El-Benna et al., 2009). This study further showed that a point mutation of the second SH3 domain or p47phox phosphorylation induced a transition from a closed to an open conformation that binds membranes through the PX domain (Marcoux et al., 2010). Our structural analysis using both crystallography and SPR techniques allows us to propose two plausible molecular models for the physical association between the interdomain-connecting loop domain of PCNA and the PX domain of p47phox. Interestingly, the p47phox 106–127 peptide that we have identified as the PCNA-interacting site in the PX domain has been previously reported to strongly inhibit NADPH oxidase activation in a cell-free system by using a peptide-walking technique to map p47phox functional domains (Morozov et al., 1998), confirming that this p47phox sequence indeed has a functional role in the control of NOX2 activation. Because PCNA is a trimer, it can potentially bind up to three PIP-motif–containing proteins at the same time (Boehm and Washington, 2016). Although the interdomain-connecting loop of PCNA can bind numerous PIP-box–containing proteins, other domains of PCNA are involved in the binding with partner proteins including p47phox, thereby increasing the diversity of interacting partners that PCNA can accommodate to orchestrate complex biological processes.

We have previously reported that the PCNA scaffold is dynamic and is adapted to the inflammatory state of the cell (Martin et al., 2016). Indeed, PCNA binding to procaspases and to p47phox has important consequences for cell survival and NADPH oxidase activation, respectively. Pertinently, p47phox-PCNA association by maintaining NOX2 in a resting state contributes to neutrophil survival. Nonetheless, PCNA–p47phox interaction is not essential for PCNA anti-apoptotic activity, since T2AA triggers apoptosis in inflammatory neutrophils in both WT and p47phox$^{-/-}$ mice.

Our study demonstrated for the first time that interfering with PCNA scaffold could be the basis of antioxidant and proresolution therapy in neutrophil-induced inflammation. A hallmark of

inflammatory bowel diseases including Crohn's disease and ulcerative colitis is excessive neutrophil accumulation in the colon, resulting in the release of toxic proteases and ROS (Parkos, 2016). Excess neutrophil-derived ROS participate in tissue damage in several inflammatory diseases, so inhibition of NADPH oxidase activation could represent a relevant therapeutic strategy (Lambeth et al., 2008).

The role of ROS in inflammation is complex, as they play a role in tissue damage as well as a positive role in the resolution of inflammation (Nathan and Cunningham-Bussel, 2013). Under certain circumstances, ROS may be beneficial in promoting wound healing, and NADPH oxidase defects in patients with chronic granulomatous disease (Segal et al., 2011) and in animal models (Morgenstern et al., 1997) lead to aberrant inflammation. Chemical NADPH oxidase inhibitors such as apocynin have antiinflammatory effects in arthritis models ('t Hart et al., 1990) and reduce ethanol-induced liver inflammation in mice (Gustot et al., 2006). Disrupting the gp91phox–p47phox interaction using a peptide inhibits NADPH oxidase (Rey et al., 2001). Likewise, targeting PCNA could be a strategy to dampen this neutrophil contribution to inflammation. In a therapeutic setting, chemical targeting of NADPH oxidase protein interaction potentially allows temporary and dose-dependent reduction of ROS, favoring the dampening of inflammation compared with the complete loss of NADPH oxidase function. It should be noted that in the current study along with the antiinflammatory effect, short T2AA treatment not only did not interfere with epithelial cell proliferation in TNBS-induced colitis, but it significantly enhanced epithelium regeneration. Our data strongly suggest that T2AA in this setting primarily targeted inflammatory neutrophils and did not demonstrate a negative effect on regenerating tissue at the site of inflammation. Here we show that T2AA also reduced neutrophil survival as an added antiinflammatory mechanism to limit neutrophil-mediated tissue damage, as previously demonstrated for roscovitine, a cyclin-dependent kinase inhibitor (Rossi et al., 2006). Down-regulating neutrophil activation and promoting neutrophil apoptosis represent important mechanisms in inflammation resolution (Serhan et al., 2007; Jones et al., 2016). Nonetheless, evaluation of the therapeutic value of T2AA as an antiinflammatory drug will require investigation of its effects on other models of inflammation. Notably, T2AA also did not adversely affect neutrophil progenitor survival. As previously mentioned, chemical strategies are reversible, and moderate reduction of NADPH oxidase function may provide antiinflammatory effects without compromising antipathogen function.

Cytosolic PCNA acts as a molecular "organizer" of neutrophil effector functions, coordinating apoptosis and governing neutrophil activation. Neutrophils represent a unique cellular model to elucidate the functions of cytosolic PCNA, and these findings could lead to the concept of molecular linkage of cell survival, oxidant-related processes, and metabolism that is relevant to the control of inflammation.

Materials and methods

Isolation of human neutrophils

Neutrophils were obtained from EDTA-anticoagulated blood from healthy donors in agreement with Etablissement Francais du Sang guidelines. Each donor gave written informed consent to participate in this study, which was approved by the Institut National de la Santé et de la Recherche Médicale Institutional Review Board (Paris, France). The study was conducted according to the Declaration of Helsinki. Neutrophils were isolated in LPS-free conditions by dextran sedimentation and Ficoll centrifugation as previously described (Witko-Sarsat et al., 2010).

Identification of PCNA partners by MS

Control IgG or rabbit polyclonal anti-PCNA Ab5 antibody (20 µg) was cross-linked to 50 µl of protein G Sepharose beads (Pierce) using 100 µl dimethyl pimelimidate (20 mM; Pierce) in cross-linking buffer (200 mM carbonate buffer, pH 9) for 30 min according to the manufacturer's instructions and as previously described (Borregaard et al., 1983; Ohayon et al., 2016). Proteins (200 µg) from human neutrophil cytosols were obtained by nitrogen cavitation to prevent granule rupture, preserving cytosolic proteins from artifactual proteolysis as previously described (Witko-Sarsat et al., 2010). Neutrophil cytosol was added to Sepharose beads cross-linked with anti-PCNA antibody and incubated for 2 h at 4°C. Proteins bound to the beads were recovered after extensive washing and were denatured at 95°C in reducing conditions with Laemmli buffer. Supernatants were loaded onto an SDS-PAGE gel for a short migration, and proteins were trypsin-digested in-gel. For liquid chromatography/MS protein analysis, peptides were concentrated, washed, and analyzed using a reverse-phase C18 column on a u3000 nanoHPLC connected to a Linear Trap Quadrupole-Orbitrap mass spectrometer (Thermo Fisher Scientific). LTQ MS/MS collision-induced dissociation spectra were acquired from the ≤20 most abundant ions detected in the Orbitrap MS scan. Protein identifications were performed with the Proteome discoverer 1.3 (Thermo Fisher Scientific) and with Mascot (http://www.matrixscience.com). Separate analysis was conducted and compared using MyPROMS software. The proteomic analysis was performed in the Proteomics 3P5 facility of the Cochin Institute–Paris Descartes University in Paris.

SPR

PCNA was expressed in *E. coli* and purified as previously described (Desplancq et al., 2016), except that size-exclusion chromatography was performed in 20 mM Tris, pH 7.5, 0.1 M NaCl, and 0.1 mM 2-ME. Recombinant human p47phox, p67phox, and Rac2 were produced as previously described (Raad et al., 2009). Recombinant p40phox expressed in *E. coli* was purchased from Creative Biomart. To generate the PX domain of p47phox, a truncated p47phox (residues 2–132) was produced in *E. coli* using the pGEX plasmid (generous gift of Dr. Yaffe, Massachusetts Institute of Technology, Cambridge, MA). SDS-PAGE analysis of purified recombinant proteins expressed in *E. coli* confirmed the purity and the expected molecular mass of each protein: PCNA (36 kD), p47phox (47 kD), p47phoxPX (14 kD), p67phox (67 kD), and Rac2 (22 kD). Interactions between PCNA and cytosolic proteins of the NADPH oxidase complex were studied by SPR on a Biacore T200 or a Biacore 3000 system (GE Healthcare) designed to calculate affinity and kinetic parameters. PCNA was covalently immobilized on a dextran layer

sensor chip (CM5) with 10 mM Hepes and 150 mM NaCl, pH 7.4. The recombinant proteins p47phox, p47phox PX domain, p67phox, p40phox, and Rac2 at the indicated concentrations (25–400 nM) were used as analytes in a running buffer (50 mM Tris and 150 mM NaCl, pH 7.4) and were injected at 20 µl/min for 120 s over immobilized PCNA (4,100 response units [RU]) and over a control flow cell submitted to the coupling steps without PCNA. Binding experiments were performed at 25°C. In all experiments, the specific binding signal was obtained by subtracting the background signal.

For global fitting of the full-length p47phox

We used kinetic titration on the Biacore T200 system, referred to as single-cycle kinetics, to collect binding data for kinetic analysis. This method involves sequential injections of several analyte concentrations over the ligand immobilized on the sensor chip surface without a regeneration step between successive injections. The association (k_a) and dissociation (k_d) rate constants and K_D were calculated using BIAevaluation software.

For peptides and p47phox PX domain–PCNA interactions

The running buffer was PBS, pH 7.4 (peptides), or 50 mM Tris and 150 mM NaCl, pH 7.4 (p47phox PX), and the surface was regenerated with pulses of 0.5 mM glycine, pH 3. The immobilization level for PCNA was 4,300 RU. Association phases ran for 120 s, and dissociation phases ran for 120 s on a Biacore 3000 system.

Inhibition assays

The phospholipid phosphatidylinositol (3,4,5)-trisphosphate (PIP3,4,5; Sigma-Aldrich), which specifically binds to the PX domain of p47phox, was used to inhibit the binding of p47phox to PCNA at the indicated concentrations ranging from 4 to 80 µM. The dose-dependent inhibition by the phospholipid PIP3,4,5 was performed on 4,100 RU of immobilized PCNA using the Biacore T200 apparatus. The solution containing p47phox (200 nM) was incubated for 10 min at 25°C with lipids at various concentrations before injection. The signal was measured at the end of the association phase (120 s) and compared with those obtained in the absence of lipids.

Inhibition studies using p21 peptide and p47phox peptides were performed using the Biacore 3000 on 2,600 RU of immobilized PCNA. p47phox (500 nM) samples were coinjected with peptides at various concentrations, and the association phase ran for 120 s. Because peptides interact with PCNA, we evaluated inhibition by measuring the SPR signal at the end of an extended dissociation phase (380 s), a time point at which peptides that have a higher dissociation rate than the protein are completely dissociated and, consequently, at which the signal is due to P47phox only. Inhibition was then evaluated by comparing the remaining signal in the dissociation phase obtained when peptide and protein were coinjected to those measured after injection of the protein alone.

Kinetic values determination

Data were analyzed by global fitting to binding models of both the association and the dissociation phases for several concentrations simultaneously using BIAevaluation software. The simplest 1:1 Langmuir binding model was first tested. The two-state reaction model and heterogeneous ligand model were used when they significantly increased the statistical goodness-of-fit as calculated by Biacore software. In the case of P47–PCNA interaction, the two-state reaction model suggested a possible conformational change of P47 during interaction. For short peptides that are supposed to be homogeneous in solution, the heterogeneous ligand model accounts for the presence of two sites that bind analyte independently of each other. SPR analysis was performed at the Structural Biology Institute at the Grenoble Instruct–European Research Infrastructure Consortium facility in Grenoble.

Crystallographic data collection and structure determination

Crystals were obtained using hanging drop vapor-diffusion technique at 20°C and by mixing 1 µl of PCNA at 4.7 mg/ml with 1 µl of the crystallization solution in the presence or absence of p47phox-106-127 peptide (Fig. S1). A search for PCNA crystallization conditions was based on previously published conditions and systematic screening using commercial screens. The best crystals were obtained with a crystallization solution containing 19–23% PEG 3350, 0.2–0.3 M NaCl, and 0.1 M Tris-HCl, pH 8.5. Approximately 12 h before crystal freezing, 100–500 µM of p47phox-106-127 peptide was added to the crystallization drop. 25% glycerol was added to the crystallization drop to prevent ice formation, and crystals were fished out and immediately frozen in liquid nitrogen. Crystallographic data were collected at −160°C on beamlines BM30-A and ID30-A1 at the European Synchrotron Radiation Facility in Grenoble, France. Data processing was performed using the XDS package, and the PCNA structure was determined by the molecular replacement technique using PHASER and the CCP4 suite of programs. The search model used was the human PCNA (PDB entry 1AXC). The final PCNA model was obtained after several cycles of manual model building with COOT software and maximum likelihood refinement using the REFMAC5 program. The highest-resolution structure was refined against 2.8-Å data, but showed no significant electron density for the soaked peptide. The structure that showed the largest amount of (F_{obs} − F_{calc}) residual electron density, located in the vicinity of the interdomain-connecting loop, was refined at 3.22-Å resolution. No peptide could be reliably refined into this electron, and the final model accounts for only the trimeric PCNA structure. Data processing and refinement statistics are presented in Table S1.

Molecular modeling

Molecular modeling was used to propose two possible docking modes of the p47phox PX domain onto the PCNA. Models are based on the crystallographic structures of the human PCNA in complex with p21-141-160 peptide (PDB entry 1AXC) and of the human p47phox PX domain (PDB entry 1KQ6). For the first model, the 106–127 PX segment was manually modified with COOT software to have the PX 114–118 region adopting the same conformation as the 147–151 segment in p21 peptide, when bound to PCNA, with an orientation compatible with docking onto PCNA. The stereochemistry of the 106–127 PX segment was

optimized by the refinement procedure implemented in COOT. The second model was built by simply superposing the PX 122–126 helix turn onto the 147–151 segment in p21 peptide, when bound to PCNA.

Transfection and differentiation of PLB985 cells

PLB985 cell lines were cultured in RPMI supplemented with 10% FBS, L-glutamine (2 mM), antibiotics (penicillin 100 U/ml and streptomycin at 100 µg/ml), and Hepes buffer. PLB985 cell granulocytic differentiation was induced by exposure to 0.5% DMF for 5 d and was validated by FACS analysis of CD11b expression, as described previously (De Chiara et al., 2013). For PCNA overexpression, PLB985 cells were stably transfected with empty pcDNA3 plasmid (pCT), pcDNA3-PCNA (PCNA), and pcDNA3-SV40NLS-PCNA (PCNA-NLS; Bouayad et al., 2012) to generate control PLB985, PLB985 overexpressing PCNA WT, and PLB985 overexpressing exclusive nuclear PCNA, respectively. For p21/waf1 overexpression, PLB985 cells were stably transfected with empty PRC-RSV-neo plasmid (Invitrogen) or PRC-RSV/p21A45R to generate control PLB985, PLB985P21, and PLB985P21A45R as previously described (Dublet et al., 2005). Notably, because p21/waf1 is sensitive to degradation by neutrophil proteinase 3, we have used the mutant p21A45R, which is resistant to serine proteases and is more stable in the current study (Martin et al., 2016). Western blot analysis using anti-PCNA (rabbit polyclonal Ab5) or p21/waf1 (rabbit polyclonal Santa Cruz) on PLB985 lysate was used to assess the expression of PCNA and p21/waf1, respectively. PCNA, p21/waf1, and actin bands were quantified and normalized as PCNA/β-actin ratio. Of note, the PCNA protein expression was not affected by the ectopic expression of p21/waf1.

For PCNA siRNA experiments, PLB985 cells were treated with DMF to induce granulocytic differentiation and transfected with 1 µM siRNA (Applied Biosystems) twice at a 24-h interval (day 4 and day 5 after DMF treatment) using the Amaxa system (Lonza), according to the manufacturer's instructions. In brief, 2×10^6 cells were resuspended in 100 µl of cell line solution with 1 µg of plasmid. The cells were then electroporated and transferred to culture plates. Transfected cells were cloned and selected based on their resistance to 1 mg/ml neomycin. FITC-conjugated control siRNA, used to detect intracellular siRNA by FACS and to monitor transfection efficiency, showed that the fluorescent siRNA was taken up in >90% of the PLB985 cells. Western blot analysis using anti-PCNA (rabbit polyclonal Ab5) on PLB985 lysate was used to validate the efficacy of PCNA siRNA in decreasing the expression of PCNA protein. PCNA and actin bands were quantified and normalized as PCNA/β-actin ratio. Flow cytometry analysis was performed at Cytometry and Immunobiology at the Cochin Institute in Paris.

Measurement of NADPH oxidase activation and ROS production in cells

Intracellular ROS accumulation in PLB985 cells was measured using DCF-DA (Sigma-Aldrich), a green fluorescent probe. DMF-differentiated PLB985 cells (0.5×10^{-6}) were prestained at 37°C for 15 min with 0.5 µM of H_2DCF-DA, which is rapidly oxidized to highly fluorescent DCF in the presence of intracellular H_2O_2. Cells were washed and stimulated for 45 min with or without PMA (1 µg/ml) at 37°C. DCF fluorescence was measured by a FACS BD Accuri C6 (BD Biosciences).

ROS production was measured by luminol CL: isolated neutrophils (1×10^5) were suspended in 0.1 ml of HBSS containing 10 µM luminol and pretreated with or without T2AA (Inoue et al., 2014; generous gift of Prof. Naoki Fujii, St. Jude Children's Research Hospital, Memphis, TN) at 10, 25, or 50 µM for 1 h at 37°C. Neutrophils were then stimulated with or without PMA (0.1 µg/ml), OZ (1 mg/ml), or f-MLF (1 µM). CL was recorded at 37°C in a luminometer (Berthold-Biolumat LB937) in duplicate over 40 min and expressed as integrated total counts. Measurement of NADPH oxidase activation in PLB985 transfected cells was performed with the same protocol except that they were adjusted at 0.5×10^{-6} cells/ml and stimulated with PMA at 1 µg/ml or OZ at 0.5 mg/ml. Luminescence was recorded using the TriStar LB 941 Multimode Microplate Reader (Berthold) and expressed as relative light units.

Measurement of NADPH oxidase activation using cell-free system experiments

NADPH oxidase activity was measured in a cell-free system using membrane and cytosolic fractions of resting neutrophils as previously described (Molshanski-Mor et al., 2007). The reaction mixture contained 1 mM ATP, 1.25 mM EGTA, 50 µM guanosine 5′-(γ-thio)triphosphate (Sigma-Aldrich), and 7×10^6 cell membrane equivalent. When indicated, the p21 peptide or T2AA was preincubated for 10 min at 37°C at the indicated concentration. Cells were then stimulated with (S) or without (R) 100 µM Li-SDS (Fluka) for 5 min at 37°C before starting the reaction. The reaction was then initiated with 200 µM β-NADPH (Sigma-Aldrich) and cytochrome c (1 mg/ml). Absorbance at 550 nm was read immediately, and superoxide anion production was calculated using an extinction coefficient of 21.1 mM^{-1} cm^{-1} for reduced ferricytochrome c. The specificity of the reaction was evaluated by adding 20 µM DPI or 30 U/ml SOD. Results are expressed as nanomoles of O_2^-/min/7×10^6 cell membrane equivalent.

Translocation of p47phox from the cytosol to the neutrophil membrane

After isolation from whole blood, 100×10^6 neutrophils were resuspended in 5 ml of $HBSS^{+/+}$ and incubated with or without T2AA (25 or 50 µM) at 37°C for 1 h. Neutrophils were then stimulated with PMA (200 ng/ml) for 8 min while the mixture was gently shaken. Ice-cold buffer was added, and cells were pelleted by centrifugation at 400 *g* for 8 min at 4°C. The pellets were resuspended in relaxation buffer containing 1 mM ATP, 1 mM EGTA, 0.5 mM PMSF, 25 nM Calyculin, and 5 µg/ml of aprotinin, leupeptin, and pepstatin. The cells were then disrupted by sonication (twice for 10 s each time) at 4°C and centrifuged at 400 *g* for 8 min. The postnuclear supernatant was loaded onto a discontinuous sucrose gradient (35 and 15% sucrose) diluted in relaxation buffer and centrifuged for 45 min at 150,000 *g*. The cytosolic and membrane fractions (in the upper and the intermediate layers, respectively) were collected. Proteins were analyzed by Western blot analysis using

anti-p47phox (BD Transduction Laboratories), anti-p22phox (Santa Cruz), anti-phospho-p47phox, and anti-PCNA (clone PC10; Santa Cruz) mouse mAbs. Expression of p22phox and total p47phox served as a loading control in membrane fraction and cytosolic fraction, respectively.

Analysis of in situ interaction between PCNA and p47phox using indirect immunofluorescence and the Duolink system

Neutrophils were spotted using round-shaped filter paper on poly-L-lysine–coated glass slides and allowed to dry in a humid chamber by gravity sedimentation, then fixed with 2% paraformaldehyde for 10 min, permeabilized with 0.2% Tween 20 for 15 min at 37°C, and blocked with 5% BSA in PBS. Cells were then incubated overnight at 4°C with a rabbit anti-PCNA polyclonal antibody (1:200) and mouse anti-p47phox mAb (1:200) diluted in 1% BSA/PBS. After washing, cells were incubated with Alexa Fluor 488–conjugated (green) goat anti-rabbit antibody (1:200) and Alexa Fluor 568–conjugated (red) goat anti-mouse antibody (1:200) for 1 h at room temperature in the dark. Nuclei were stained with TO-PRO-3 iodide (Invitrogen). A proximity ligation assay using the Duolink system was performed on human isolated neutrophils spotted on poly-L-lysine–coated glass slides according to the manufacturer's instructions using two primary antibodies from different species (the rabbit polyclonal anti-PCNA Ab5, the mAb anti-p47phox [Millipore], or the rabbit polyclonal anti-rac 2 [Abcam]). When indicated, neutrophils were treated with PMA (0.1 µg/ml for 10 min) before labeling. Resting neutrophils treated with anti-p47phox; anti-PCNA antibodies show a cytosolic fluorescence indicative of a colocalization. Hoechst was used for nuclear staining. Stained cells were examined with a Zeiss LSM510 confocal microscope (63×/1.4 numerical aperture objective), and the images were imported into an LSM image browser for analysis. The designation "merge" for indirect immunofluorescence analysis corresponds to colocalization of PCNA and p47phox. The magnification used was 63×, and different zoom settings were used. The final magnification is indicated by the presence of a scale bar for each experiment.

Coimmunoprecipitation experiments

Human isolated neutrophils (25 × 10^6/ml per condition) were stimulated with PMA (0.1 µg/ml) or f-MLF (1 µM) for 1 h at 37°C with 5% CO_2. Neutrophil cytosol was obtained by sonication in a hypotonic Hepes buffer (50 mM) supplemented with inhibitors (4 mM PMSF, 20 mM leupeptin, 20 mM pepstatin, 270 mM orthovanadate, 200 mM EGTA, and 500 mM EDTA) with a Soniprep 150 Plus sonicator (1 Hz for 10 s). Protein concentration was measured using the BCA kit (Pierce). Coimmunoprecipitation experiments were performed on cytosol (500 µg of protein) by adding 7.5 µl rabbit anti-PCNA Ab5 or control rabbit IgG for 15 min at 4°C under rolling. Next, 50 µl of protein A beads were added and incubated for 30 min at 4°C under rolling and 15 min on ice. The sample was loaded onto a column containing Sepharose-coated magnetic beads (Miltenyi) prehydrated with a washing buffer (50 mM Tris, pH 8, 300 mM NaCl, and 1% NP-40). The column was washed four times with this salt-containing buffer and five times with a wash buffer (20 mM Tris, pH 7.5). The sample was eluted from the column with 50 µl 5× boiling sample buffer. Cytosol (30 µg of protein) elution and exclusion samples were analyzed by Western blotting using anti-p47phox (BD Biosciences; 610354) and PCNA (PC10 mAb) followed by HRP-conjugated anti-mouse IgG (Nordic Immunology; diluted 1:5,000), using the SuperSignal West Pico detection kit (Pierce) as previously described (Witko-Sarsat et al., 2010).

Mouse models of inflammation

Animal studies were performed in accordance with the European Community Guidelines (authorization number B-75-1394 and C-75-1801). All protocols were approved by Ethics Committee for Animal Research of Université Paris Descartes (CEEA34-VWS.074.12) and of Faculté Bichat (CEEA-JCM.121).

Zymosan-induced peritonitis in mice

The model of zymosan-induced peritonitis was used to examine the NADPH oxidase activity in murine inflammatory neutrophils. Peritonitis was induced in mice (male C57BL/6J mice, 9–30 wk old; Charles River) by an intraperitoneal injection of 1 mg of Zymosan A from *Saccharomyces cerevisiae* (40 mg/kg; Sigma-Aldrich) in 0.5 ml of sterile PBS as previously described (Martin et al., 2016). After 4 h, mice were sacrificed by cervical dislocation, and the peritoneal cavities were washed with 4 ml of PBS. Aliquots of lavage fluids (10 µl) were diluted in Turk's solution (0.01% crystal violet in 3% acetic acid), and cells were counted using a Mallassez hemocytometer. Analysis of neutrophils or macrophages was performed by flow cytometry after immunolabeling with anti-Ly6G-FITC (BD Biosciences) and anti-F4/80–Alexa Fluor 647 (AbD Serotec), respectively. Isolated neutrophils (1 × 10^6) from the peritoneal lavage were suspended in 0.5 ml $HBSS^{+/+}$ and stimulated with or without PMA (1 µg/ml), and luminol CL was recorded by a TriStar LB 941 Multimode Microplate Reader as described above. When indicated, zymosan-induced peritonitis was performed in p21/Waf1 knockout mice ($p21^{-/-}$) obtained from the Jackson Laboratory (B6;129S2-Cdkn1atm1Tyj/J) and housed with their WT littermate controls (Martin et al., 2016). To evaluate the effect of in vivo injection of T2AA on oxidative burst in inflammatory neutrophils, mice were pretreated with or without T2AA (20 mg/kg) for 30 min and 17 h before the injection of zymosan to trigger peritonitis.

To evaluate the ex vivo effect of T2AA on the survival of neutrophils in C57BL/6J WT mice compared with mice lacking p47phox ($p47phox^{-/-}$ mice [$Ncf1^{m1J}$]; the Jackson Laboratory), peritonitis was induced in mice (male and female C57BL/6J mice, 9–30 wk old) by an intraperitoneal injection of zymosan. After 4 h, mice were sacrificed with isoflurane, and the peritoneal cavities were washed with 4 ml of PBS. Neutrophils were then purified using a Ficoll gradient and cultured at 37°C in 5% CO_2 for 16 h with or without T2AA (10, 25, or 50 µM). Next, 0.2 × 10^5 of purified neutrophils in basal state and after overnight incubation were stained with APC-conjugated mAb anti-Ly6G (BD Pharmigen; clone 1A8; 4 µg/ml final concentration) and also FITC-conjugated Annexin-V (Miltenyi Biotec) and 7-aminoactinomycin D (7-AAD; BD Biosciences) to evaluate the proportion of neutrophil survival.

Induction of TNBS-induced colitis in mice

We investigated the therapeutic effect of T2AA in TNBS-induced colitis in mice as previously described (Krimi et al., 2008). Male C57BL/6J mice (19–22 g; Janvier Laboratories) were deprived of food for 24 h before colitis induction. Then mice were anesthetized for 90–120 min for the induction of colitis. They received an intrarectal administration of TNBS (40 µl, 150 mg/kg) dissolved in a 1:1 mixture of 0.9% NaCl with 100% ethanol. Control mice received a 1:1 mixture of 0.9% NaCl with 100% ethanol. After each rectal administration of TNBS, mice were kept in an inverted position for 30 s. 6 and 24 h after TNBS injection, mice received an intraperitoneal injection of T2AA (25 mg/kg) or vehicle solution. Animals were sacrificed 2 d after TNBS administration. When indicated, neutrophil depletion was performed using two injections of anti-Ly6G antibody (clone 1A8) as previously described (Coffelt et al., 2015), 18 h (400 µg/mouse) before and 5 h (100 µg/mouse) after induction of colitis (Fig. 8 A).

Colic inflammation was evaluated by the weight and length of each intestine (anus to cecum). The colons were opened and examined to evaluate macroscopic lesions according to the Wallace criteria (Wallace et al., 1989). The Wallace score rates macroscopic lesions on a scale from 0 to 10 based on features reflecting inflammation such as hyperemia, thickening of the bowel, and extent of ulceration. For histological analysis, colon specimens located 1 cm above the anus were removed to be included in paraffin. Several 5-µm paraffin sections were prepared and stained with H&E according to the Ameho criteria (Ameho et al., 1997). This grading is scaled from 0 to 6 and takes into account the presence of erosion, ulceration, or necrosis and the depth and surface of lesions. Immunohistological labeling of colon sections was also performed with a polyclonal rabbit anti-MPO (A0398, Dako) and with the neutrophil-specific marker antibody (rat mAb clone 6A608; Santa Cruz) as previously described (Martin et al., 2016). To evaluate the presence of neutrophils within the colon, we quantified the immunostaining obtained with the neutrophil marker (clone 6A608). Slides were entirely scanned by the Lamina Slide Scanner (PerkinElmer), and regions of interest were manually defined using Case Viewer (https://www.3dhistech.com/software-downloads). Surfaces of tissue regions of interest were determined with INFORM software (PerkinElmer) by tissue segmentation. Then, surfaces of neutrophil signal were determined by the "threshold" command. The ratio between these two surfaces were calculated to analyze and compare the variations of the immunostained surfaces percentage. The immunohistochemistry study was performed at the Histology, Immunostaining, and Laser Microdissection facility at Cochin Institute in Paris.

Noninvasive in vivo imaging of NADPH oxidase activity using L012-enhanced CL

Measurement of in vivo neutrophil NADPH activation was performed as previously described (Kielland et al., 2009), with some modifications. For the zymosan-induced peritonitis model, mice were first injected intraperitoneally with 1 mg zymosan to induce peritonitis, followed by T2AA treatment (25 mg/kg) 4 h later. To measure in vivo neutrophil NADPH activation, the luminescent probe L012 (Sobioda) was prepared freshly right before the experiment by dissolving 2 mg L012/ml in sterile PBS and kept in the dark. L012 was administered at 20 mg/kg by intraperitoneal injection to the right flank of isofluorane-anesthetized (1.5–2.5%) mice 6 h after the initial injection of zymosan. In the model of TNBS-induced colitis, L012 was injected at 24 and 48 h after TNBS treatment to measure in vivo activity of NADPH oxidase at these time points. Results are expressed as the variation of L012-CL between 24 and 48 h. For all the in vivo imaging of NADPH oxidase activity, L012 was administered to mice that had been under anesthesia for 3 to 4 min, after which mice were placed into the light chamber of the Photon Imager RT imaging system (BiospaceLab) equipped with an intensified charge-coupled device camera that allows real-time recording of emitted photons. The number of photons produced by L012 during in vivo imaging was collected during 10 min. A maximum of five individual mice per acquisition were positioned supine in the chamber. Regions of interest were drawn using M3 Vision proprietary software (BiospaceLab). This software allows quantification of photons emitted over time in each region of interest with real-time photon collection. Quantification was performed measuring emitted photons in a time window corresponding to the plateau of the intensity curve, for each region of interest. Light emission from the abdominal region of interest was quantified and expressed as photons/s/cm^2/steradian. This study was performed at the Small Animal Imaging facility at the Cochin Institute in Paris.

Statistical analysis

Statistical analysis was performed using the Statview software package. Comparisons were made using the Student's *t* test, multicomparison ANOVA, or the Mann–Whitney *U* test as indicated. Differences were considered significant at $P < 0.05$.

Accession numbers

The structure factors and coordinates have been deposited in the PDB under accession nos. 6FCM (PCNA structure at 2.8 Å) and 6FCN (PCNA structure at 3.22 Å in combination with the p47phox peptide).

Online supplemental material

Fig. S1 is a structural analysis of the association between PCNA and the p47phox peptides. Fig. S2 shows the effect of PCNA inhibition on viability in differentiated PLB985 cells or human neutrophils. Fig. S3 shows the effect of T2AA on degranulation, chemotaxis, and phagocytosis of *E. coli* in isolated human neutrophils. Fig. S4 shows the effect of T2AA on neutrophil survival isolated from WT and from p47phox$^{-/-}$ mice. Table S1 shows crystallographic data collection and refinement statistics.

Acknowledgments

The authors acknowledge Dr. Naoki Fujii for useful comments on the manuscript; the Cochin Institute proteomic 3P5, flow cytometry, and animal care facilities; the Etablissement Français du Sang; the European Synchrotron Radiation Facility; and the SPR platform Grenoble Instruct–European Research Infrastructure Consortium center (ISBG UMS-3518-CNRS-CEA-UGA-EMBL).

Funding was provided by LabEx INFLAMEX (ANR-11-IDEX-0005-02 Sorbonne Paris Cité to V. Witko-Sarsat and J. El-Benna). V. Witko-Sarsat was funded by the Départements Hospitalo Universitaires–Autoimmune and hormonal diseases (Assistance Publique–Hôpitaux de Paris Université Paris Descartes), Chancellerie des Universités de Paris; Association Vaincre la Mucoviscidose (PhD fellowship; D. Ohayon); ABCF Mucoviscidose; Association pour la Recherche sur le Cancer (ARC-PJA-20131200141); and Arthritis Foundation. P. Frachet and D. Housset were funded by Agence Nationale de la Recherche (ANR-FRISBI-10-INSB-05-02 and GRAL-ANR-10-LABX-49-01) and the Grenoble Partnership for Structural Biology. C. Benarafa was funded by the Swiss National Science Foundation (310030-173137). G. Renault was supported by France Life Imaging (Agence Nationale de la Recherche grant ANR-11-INBS-0006).

The authors declare no competing financial interests.

Author contributions: A. De Chiara, C. Candalh, D. Ohayon, J. Mocek, and P.M.C. Dang conducted and analyzed experiments; S.S. Burgener, and C. Benarafa generated p47phox$^{-/-}$ data; V. Marzaioli, F. Walker, M. Favier, and C. Pintard performed histopathology and immunolabeling; D. Desplancq and E. Weiss produced proteins in *E. coli*; G. Renault and I. Lagoutte performed in vivo imaging; P. Tacnet-Delorme, D. Housset, and P. Frachet generated SPR and crystallography data; J-C. Marie and J. El-Benna designed colitis experiments; D. Ohayon, P.M.C. Dang, E. Weiss, D. Housset, J-C. Marie, P. Frachet, J. El-Benna, N. Thieblemont, S. Chatfield, and M. Hurtado-Nedelec participated in data analysis, experiments for the revised version, and manuscript writing. V. Witko-Sarsat supervised the project and wrote the manuscript. All authors read and approved the manuscript.

Submitted: 25 February 2018
Revised: 17 June 2019
Accepted: 16 August 2019

References

't Hart, B.A., J.M. Simons, S. Knaan-Shanzer, N.P. Bakker, and R.P. Labadie. 1990. Antiarthritic activity of the newly developed neutrophil oxidative burst antagonist apocynin. *Free Radic. Biol. Med.* 9:127–131. https://doi.org/10.1016/0891-5849(90)90115-Y

Ameho, C.K., A.A. Adjei, E.K. Harrison, K. Takeshita, T. Morioka, Y. Arakaki, E. Ito, I. Suzuki, A.D. Kulkarni, A. Kawajiri, and S. Yamamoto. 1997. Prophylactic effect of dietary glutamine supplementation on interleukin 8 and tumour necrosis factor alpha production in trinitrobenzene sulphonic acid induced colitis. *Gut.* 41:487–493. https://doi.org/10.1136/gut.41.4.487

Baillet, A., M.A. Hograindleur, J. El Benna, A. Grichine, S. Berthier, F. Morel, and M.H. Paclet. 2017. Unexpected function of the phagocyte NADPH oxidase in supporting hyperglycolysis in stimulated neutrophils: key role of 6-phosphofructo-2-kinase. *FASEB J.* 31:663–673. https://doi.org/10.1096/fj.201600720R

Boehm, E.M., and M.T. Washington. 2016. R.I.P. to the PIP: PCNA-binding motif no longer considered specific: PIP motifs and other related sequences are not distinct entities and can bind multiple proteins involved in genome maintenance. *BioEssays.* 38:1117–1122. https://doi.org/10.1002/bies.201600116

Borregaard, N., J.M. Heiple, E.R. Simons, and R.A. Clark. 1983. Subcellular localization of the b-cytochrome component of the human neutrophil microbicidal oxidase: translocation during activation. *J. Cell Biol.* 97:52–61. https://doi.org/10.1083/jcb.97.1.52

Bouayad, D., M. Pederzoli-Ribeil, J. Mocek, C. Candalh, J.B. Arlet, O. Hermine, N. Reuter, N. Davezac, and V. Witko-Sarsat. 2012. Nuclear-to-cytoplasmic relocalization of the proliferating cell nuclear antigen (PCNA) during differentiation involves a chromosome region maintenance 1 (CRM1)-dependent export and is a prerequisite for PCNA anti-apoptotic activity in mature neutrophils. *J. Biol. Chem.* 287:33812–33825. https://doi.org/10.1074/jbc.M112.367839

Boussetta, T., M.A. Gougerot-Pocidalo, G. Hayem, S. Ciappelloni, H. Raad, R. Arabi Derkawi, O. Bournier, Y. Kroviarski, X.Z. Zhou, J.S. Malter, et al. 2010. The prolyl isomerase Pin1 acts as a novel molecular switch for TNF-alpha-induced priming of the NADPH oxidase in human neutrophils. *Blood.* 116:5795–5802. https://doi.org/10.1182/blood-2010-03-273094

Coffelt, S.B., K. Kersten, C.W. Doornebal, J. Weiden, K. Vrijland, C.S. Hau, N.J.M. Verstegen, M. Ciampricotti, L.J.A.C. Hawinkels, J. Jonkers, and K.E. de Visser. 2015. IL-17-producing γδ T cells and neutrophils conspire to promote breast cancer metastasis. *Nature.* 522:345–348. https://doi.org/10.1038/nature14282

De Chiara, A., M. Pederzoli-Ribeil, J. Mocek, C. Candalh, P. Mayeux, A. Millet, and V. Witko-Sarsat. 2013. Characterization of cytosolic proliferating cell nuclear antigen (PCNA) in neutrophils: antiapoptotic role of the monomer. *J. Leukoc. Biol.* 94:723–731. https://doi.org/10.1189/jlb.1212637

Desplancq, D., G. Freund, S. Conic, A.P. Sibler, P. Didier, A. Stoessel, M. Oulad-Abdelghani, M. Vigneron, J. Wagner, Y. Mély, et al. 2016. Targeting the replisome with transduced monoclonal antibodies triggers lethal DNA replication stress in cancer cells. *Exp. Cell Res.* 342:145–158. https://doi.org/10.1016/j.yexcr.2016.03.003

Dublet, B., A. Ruello, M. Pederzoli, E. Hajjar, M. Courbebaisse, S. Canteloup, N. Reuter, and V. Witko-Sarsat. 2005. Cleavage of p21/WAF1/CIP1 by proteinase 3 modulates differentiation of a monocytic cell line. Molecular analysis of the cleavage site. *J. Biol. Chem.* 280:30242–30253. https://doi.org/10.1074/jbc.M414609200

El-Benna, J., P.M. Dang, M.A. Gougerot-Pocidalo, J.C. Marie, and F. Braut-Boucher. 2009. p47phox, the phagocyte NADPH oxidase/NOX2 organizer: structure, phosphorylation and implication in diseases. *Exp. Mol. Med.* 41:217–225. https://doi.org/10.3858/emm.2009.41.4.058

El-Benna, J., M. Hurtado-Nedelec, V. Marzaioli, J.C. Marie, M.A. Gougerot-Pocidalo, and P.M. Dang. 2016. Priming of the neutrophil respiratory burst: role in host defense and inflammation. *Immunol. Rev.* 273:180–193. https://doi.org/10.1111/imr.12447

Geering, B., and H.U. Simon. 2011. Peculiarities of cell death mechanisms in neutrophils. *Cell Death Differ.* 18:1457–1469. https://doi.org/10.1038/cdd.2011.75

Gulbis, J.M., Z. Kelman, J. Hurwitz, M. O'Donnell, and J. Kuriyan. 1996. Structure of the C-terminal region of p21(WAF1/CIP1) complexed with human PCNA. *Cell.* 87:297–306. https://doi.org/10.1016/S0092-8674(00)81347-1

Gustot, T., A. Lemmers, C. Moreno, N. Nagy, E. Quertinmont, C. Nicaise, D. Franchimont, H. Louis, J. Devière, and O. Le Moine. 2006. Differential liver sensitization to toll-like receptor pathways in mice with alcoholic fatty liver. *Hepatology.* 43:989–1000. https://doi.org/10.1002/hep.21138

Inoue, A., S. Kikuchi, A. Hishiki, Y. Shao, R. Heath, B.J. Evison, M. Actis, C.E. Canman, H. Hashimoto, and N. Fujii. 2014. A small molecule inhibitor of monoubiquitinated Proliferating Cell Nuclear Antigen (PCNA) inhibits repair of interstrand DNA cross-link, enhances DNA double strand break, and sensitizes cancer cells to cisplatin. *J. Biol. Chem.* 289:7109–7120. https://doi.org/10.1074/jbc.M113.520429

Iyer, S.S., D.W. Pearson, W.M. Nauseef, and R.A. Clark. 1994. Evidence for a readily dissociable complex of p47phox and p67phox in cytosol of unstimulated human neutrophils. *J. Biol. Chem.* 269:22405–22411.

Jones, H.R., C.T. Robb, M. Perretti, and A.G. Rossi. 2016. The role of neutrophils in inflammation resolution. *Semin. Immunol.* 28:137–145. https://doi.org/10.1016/j.smim.2016.03.007

Kanai, F., H. Liu, S.J. Field, H. Akbary, T. Matsuo, G.E. Brown, L.C. Cantley, and M.B. Yaffe. 2001. The PX domains of p47phox and p40phox bind to lipid products of PI(3)K. *Nat. Cell Biol.* 3:675–678. https://doi.org/10.1038/35083070

Karathanassis, D., R.V. Stahelin, J. Bravo, O. Perisic, C.M. Pacold, W. Cho, and R.L. Williams. 2002. Binding of the PX domain of p47(phox) to phosphatidylinositol 3,4-bisphosphate and phosphatidic acid is masked by an intramolecular interaction. *EMBO J.* 21:5057–5068. https://doi.org/10.1093/emboj/cdf519

Kasahara, Y., K. Iwai, A. Yachie, K. Ohta, A. Konno, H. Seki, T. Miyawaki, and N. Taniguchi. 1997. Involvement of reactive oxygen intermediates in spontaneous and CD95 (Fas/APO-1)-mediated apoptosis of neutrophils. *Blood.* 89:1748–1753.

Kennedy, A.D., and F.R. DeLeo. 2009. Neutrophil apoptosis and the resolution of infection. *Immunol. Res.* 43:25–61. https://doi.org/10.1007/s12026-008-8049-6

Kielland, A., T. Blom, K.S. Nandakumar, R. Holmdahl, R. Blomhoff, and H. Carlsen. 2009. In vivo imaging of reactive oxygen and nitrogen species in inflammation using the luminescent probe L-012. *Free Radic. Biol. Med.* 47:760–766. https://doi.org/10.1016/j.freeradbiomed.2009.06.013

Krimi, R.B., L. Kotelevets, L. Dubuquoy, P. Plaisancié, F. Walker, T. Lehy, P. Desreumaux, I. Van Seuningen, E. Chastre, M.E. Forgue-Lafitte, and J.C. Marie. 2008. Resistin-like molecule beta regulates intestinal mucous secretion and curtails TNBS-induced colitis in mice. *Inflamm. Bowel Dis.* 14:931–941. https://doi.org/10.1002/ibd.20420

Lambeth, J.D., K.H. Krause, and R.A. Clark. 2008. NOX enzymes as novel targets for drug development. *Semin. Immunopathol.* 30:339–363. https://doi.org/10.1007/s00281-008-0123-6

Maga, G., and U. Hubscher. 2003. Proliferating cell nuclear antigen (PCNA): a dancer with many partners. *J. Cell Sci.* 116:3051–3060. https://doi.org/10.1242/jcs.00653

Mantovani, A., M.A. Cassatella, C. Costantini, and S. Jaillon. 2011. Neutrophils in the activation and regulation of innate and adaptive immunity. *Nat. Rev. Immunol.* 11:519–531. https://doi.org/10.1038/nri3024

Marcoux, J., P. Man, I. Petit-Haertlein, C. Vivès, E. Forest, and F. Fieschi. 2010. p47phox molecular activation for assembly of the neutrophil NADPH oxidase complex. *J. Biol. Chem.* 285:28980–28990. https://doi.org/10.1074/jbc.M110.139824

Martin, C., D. Ohayon, M. Alkan, J. Mocek, M. Pederzoli-Ribeil, C. Candalh, G. Thevenot, A. Millet, N. Tamassia, M.A. Cassatella, et al. 2016. Neutrophil-Expressed p21/waf1 Favors Inflammation Resolution in *Pseudomonas aeruginosa* Infection. *Am. J. Respir. Cell Mol. Biol.* 54:740–750. https://doi.org/10.1165/rcmb.2015-0047OC

Moldovan, G.L., B. Pfander, and S. Jentsch. 2007. PCNA, the maestro of the replication fork. *Cell.* 129:665–679. https://doi.org/10.1016/j.cell.2007.05.003

Molshanski-Mor, S., A. Mizrahi, Y. Ugolev, I. Dahan, Y. Berdichevsky, and E. Pick. 2007. Cell-free assays: the reductionist approach to the study of NADPH oxidase assembly, or "all you wanted to know about cell-free assays but did not dare to ask". *Methods Mol. Biol.* 412:385–428. https://doi.org/10.1007/978-1-59745-467-4_25

Morgenstern, D.E., M.A. Gifford, L.L. Li, C.M. Doerschuk, and M.C. Dinauer. 1997. Absence of respiratory burst in X-linked chronic granulomatous disease mice leads to abnormalities in both host defense and inflammatory response to Aspergillus fumigatus. *J. Exp. Med.* 185:207–218. https://doi.org/10.1084/jem.185.2.207

Morozov, I., O. Lotan, G. Joseph, Y. Gorzalczany, and E. Pick. 1998. Mapping of functional domains in p47(phox) involved in the activation of NADPH oxidase by "peptide walking". *J. Biol. Chem.* 273:15435–15444. https://doi.org/10.1074/jbc.273.25.15435

Nathan, C., and A. Cunningham-Bussel. 2013. Beyond oxidative stress: an immunologist's guide to reactive oxygen species. *Nat. Rev. Immunol.* 13:349–361. https://doi.org/10.1038/nri3423

Nauseef, W.M. 2007. How human neutrophils kill and degrade microbes: an integrated view. *Immunol. Rev.* 219:88–102. https://doi.org/10.1111/j.1600-065X.2007.00550.x

Ohayon, D., A. De Chiara, N. Chapuis, C. Candalh, J. Mocek, J.A. Ribeil, L. Haddaoui, N. Ifrah, O. Hermine, F. Bouillaud, et al. 2016. Cytoplasmic proliferating cell nuclear antigen connects glycolysis and cell survival in acute myeloid leukemia. *Sci. Rep.* 6:35561. https://doi.org/10.1038/srep35561

Park, J.W., J.E. Benna, K.E. Scott, B.L. Christensen, S.J. Chanock, and B.M. Babior. 1994. Isolation of a complex of respiratory burst oxidase components from resting neutrophil cytosol. *Biochemistry.* 33:2907–2911. https://doi.org/10.1021/bi00176a021

Parkos, C.A. 2016. Neutrophil-Epithelial Interactions: A Double-Edged Sword. *Am. J. Pathol.* 186:1404–1416. https://doi.org/10.1016/j.ajpath.2016.02.001

Punchihewa, C., A. Inoue, A. Hishiki, Y. Fujikawa, M. Connelly, B. Evison, Y. Shao, R. Heath, I. Kuraoka, P. Rodrigues, et al. 2012. Identification of small molecule proliferating cell nuclear antigen (PCNA) inhibitor that disrupts interactions with PIP-box proteins and inhibits DNA replication. *J. Biol. Chem.* 287:14289–14300. https://doi.org/10.1074/jbc.M112.353201

Raad, H., M.H. Paclet, T. Boussetta, Y. Kroviarski, F. Morel, M.T. Quinn, M.A. Gougerot-Pocidalo, P.M. Dang, and J. El-Benna. 2009. Regulation of the phagocyte NADPH oxidase activity: phosphorylation of gp91phox/NOX2 by protein kinase C enhances its diaphorase activity and binding to Rac2, p67phox, and p47phox. *FASEB J.* 23:1011–1022. https://doi.org/10.1096/fj.08-114553

Reeves, E.P., L.V. Dekker, L.V. Forbes, F.B. Wientjes, A. Grogan, D.J. Pappin, and A.W. Segal. 1999. Direct interaction between p47phox and protein kinase C: evidence for targeting of protein kinase C by p47phox in neutrophils. *Biochem. J.* 344:859–866. https://doi.org/10.1042/bj3440859

Rey, F.E., M.E. Cifuentes, A. Kiarash, M.T. Quinn, and P.J. Pagano. 2001. Novel competitive inhibitor of NAD(P)H oxidase assembly attenuates vascular O(2)(-) and systolic blood pressure in mice. *Circ. Res.* 89:408–414. https://doi.org/10.1161/hh1701.096037

Rossi, A.G., D.A. Sawatzky, A. Walker, C. Ward, T.A. Sheldrake, N.A. Riley, A. Caldicott, M. Martinez-Losa, T.R. Walker, R. Duffin, et al. 2006. Cyclin-dependent kinase inhibitors enhance the resolution of inflammation by promoting inflammatory cell apoptosis. *Nat. Med.* 12:1056–1064. https://doi.org/10.1038/nm1468

Segal, B.H., P. Veys, H. Malech, and M.J. Cowan. 2011. Chronic granulomatous disease: lessons from a rare disorder. *Biol. Blood Marrow Transplant.* 17(1, Suppl):S123–S131. https://doi.org/10.1016/j.bbmt.2010.09.008

Serhan, C.N., S.D. Brain, C.D. Buckley, D.W. Gilroy, C. Haslett, L.A. O'Neill, M. Perretti, A.G. Rossi, and J.L. Wallace. 2007. Resolution of inflammation: state of the art, definitions and terms. *FASEB J.* 21:325–332. https://doi.org/10.1096/fj.06-7227rev

Shmelzer, Z., M. Karter, M. Eisenstein, T.L. Leto, N. Hadad, D. Ben-Menahem, D. Gitler, S. Banani, B. Wolach, M. Rotem, and R. Levy. 2008. Cytosolic phospholipase A2alpha is targeted to the p47phox-PX domain of the assembled NADPH oxidase via a novel binding site in its C2 domain. *J. Biol. Chem.* 283:31898–31908. https://doi.org/10.1074/jbc.M804674200

Soehnlein, O., S. Steffens, A. Hidalgo, and C. Weber. 2017. Neutrophils as protagonists and targets in chronic inflammation. *Nat. Rev. Immunol.* 17:248–261. https://doi.org/10.1038/nri.2017.10

Wallace, J.L., W.K. MacNaughton, G.P. Morris, and P.L. Beck. 1989. Inhibition of leukotriene synthesis markedly accelerates healing in a rat model of inflammatory bowel disease. *Gastroenterology.* 96:29–36. https://doi.org/10.1016/0016-5085(89)90760-9

Warbrick, E. 1998. PCNA binding through a conserved motif. *BioEssays.* 20:195–199. https://doi.org/10.1002/(SICI)1521-1878(199803)20:3<195::AID-BIES2>3.0.CO;2-R

Warbrick, E. 2006. A functional analysis of PCNA-binding peptides derived from protein sequence, interaction screening and rational design. *Oncogene.* 25:2850–2859. https://doi.org/10.1038/sj.onc.1209320

Witko-Sarsat, V., and D. Ohayon. 2016. Proliferating cell nuclear antigen in neutrophil fate. *Immunol. Rev.* 273:344–356. https://doi.org/10.1111/imr.12449

Witko-Sarsat, V., J. Mocek, D. Bouayad, N. Tamassia, J.A. Ribeil, C. Candalh, N. Davezac, N. Reuter, L. Mouthon, O. Hermine, et al. 2010. Proliferating cell nuclear antigen acts as a cytoplasmic platform controlling human neutrophil survival. *J. Exp. Med.* 207:2631–2645. https://doi.org/10.1084/jem.20092241

Zheleva, D.I., N.Z. Zhelev, P.M. Fischer, S.V. Duff, E. Warbrick, D.G. Blake, and D.P. Lane. 2000. A quantitative study of the in vitro binding of the C-terminal domain of p21 to PCNA: affinity, stoichiometry, and thermodynamics. *Biochemistry.* 39:7388–7397. https://doi.org/10.1021/bi992498r

Supplemental material

Ohayon et al., https://doi.org/10.1084/jem.20180371

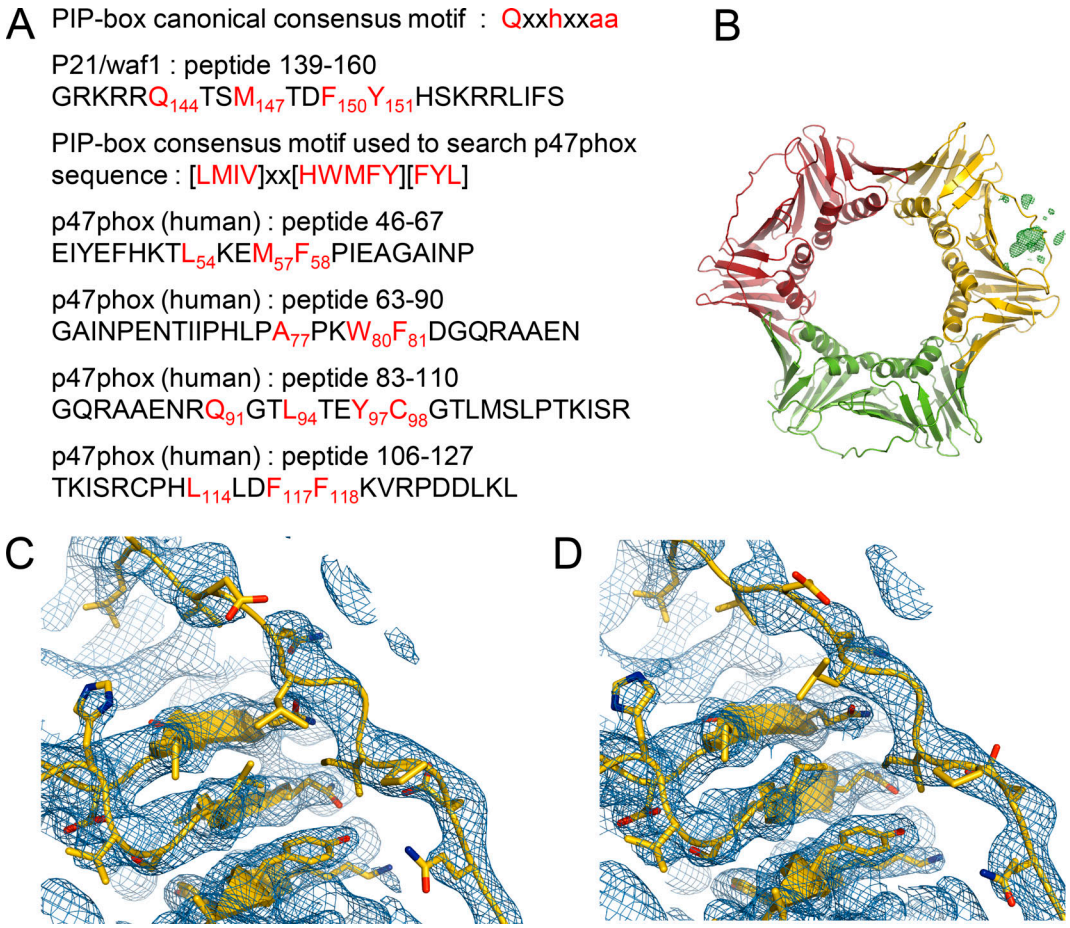


Figure S1. **Structural analysis of the association between PCNA and the p47phox peptides. (A)** Sequences of the putative PIP box on p47phox PX domain and corresponding peptides designed for SPR experiments. **(B–D)** Crystallographic data of PCNA associated with the p47phox peptide. **(B)** Schematic view of trimeric human PCNA refined at 3.23 Å, obtained with human PCNA crystals soaked in a 100-µM p47phox$_{106–127}$ peptide solution for 24 h before data collection. This experiment was performed three times with identical results. The three monomers are shown in green, yellow, and red. The main peak of the residual (F_{obs} − F_{calc}) electron density map, contoured at the +2.8 σ level, is shown in green. **(C)** ($2F_{obs}$ − F_{calc}) electron density map of the 3.23-Å-resolution structure (PDB entry code 6FCN), contoured at the +1 σ level, in the region of the interdomain-connecting loop. **(D)** ($2F_{obs}$ − F_{calc}) electron density map of the 2.80-Å-resolution structure (PDB entry code 6FCM), contoured at the +1 σ level, in the region of the interdomain-connecting loop. Of note, the analysis of the crystal packing shows that there are symmetry-related molecules in the vicinity of the interdomain-connecting loop. These symmetry mates may partially prevent peptide binding. Therefore, the soaking time has been adjusted to optimize peptide binding without affecting the crystal order. The 50 crystals tested differ in size, and also slightly in unit cell parameters (range of 37.3–40.0 Å for a axis, 138.4–140.9 Å for b axis, 164.8–172.1 Å for c axis).

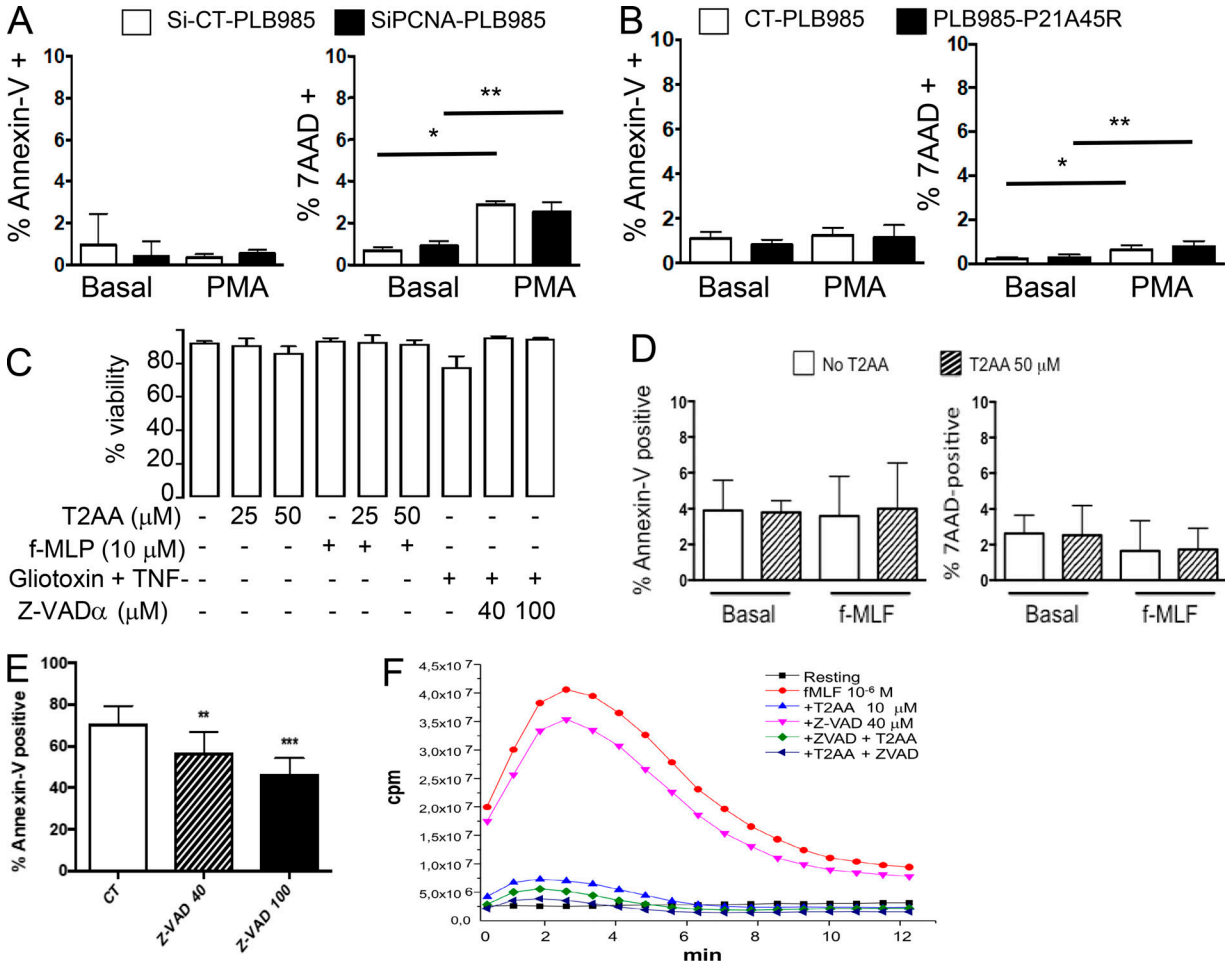


Figure S2. **The decreased oxidative burst triggered by PCNA inhibition observed in differentiated PLB985 cells or in human neutrophils is not due to decreased viability. (A and B)** Flow cytometry analysis of apoptotic and necrotic cells after labeling with Annexin-V and 7-AAD, respectively, in DMF-differentiated PLB985. **(A)** DMF-differentiated PLB985 were transfected by control siRNA or PCNA-siRNA and stimulated by PMA (1 μg/ml) for 1 h. The data are mean ± SEM; *, P < 0.05; **, P < 0.01 (ANOVA; *n* = 4). **(B)** DMF-differentiated PLB985 were transfected with either control plasmid or pcDNA/p21A45R and treated by PMA (1 μg/ml) for 1 h. The data are mean ± SEM; *, P < 0.05; **, P < 0.01 (ANOVA; *n* = 6). **(C and D)** Evaluation of viability in human neutrophils treated with T2AA in the presence or absence of f-MLF (10^{-6} M) for 1 h. Double labeling with Annexin-V and 7-AAD was performed in human isolated neutrophils treated by f-MLF. This time point was chosen because the duration of the measurement of NADPH oxidase activity was 40 min. **(C)** Viable neutrophils are double-negative neutrophils. The data are mean ± SEM; *, P < 0.05 (ANOVA) of four independent experiments with distinct blood donors (*n* = 4). **(D)** The percentage of Annexin-V and 7-AAD neutrophils represent apoptotic and necrotic neutrophils, respectively. The data are mean ± SEM. **(E)** Effect of Z-VAD at 40 and 100 μM on spontaneous apoptosis of human isolated neutrophils incubated for 16 h at 37°C. Apoptosis was evaluated by flow cytometry by the percentage of neutrophils labeled with fluorescent Annexin-V. The data are mean ± SEM; ** P < 0.01 (ANOVA test) of *n* = 6. ***, P < 0.001. **(F)** Effect of the caspase inhibitor Z-VAD on f-MLF–induced NADPH oxidase–dependent oxidant production. Luminol-amplified CL was measured in isolated neutrophils as described in Materials and methods. Isolated neutrophils were preincubated for 15 min with either 10 μM T2AA alone or a combination of T2AA plus Z-VAD (40 μM) before stimulation with f-MLF. The CL was recorded for 15 min, and a representative experiment is shown. This experiment was reproduced with two distinct healthy donors with similar results.

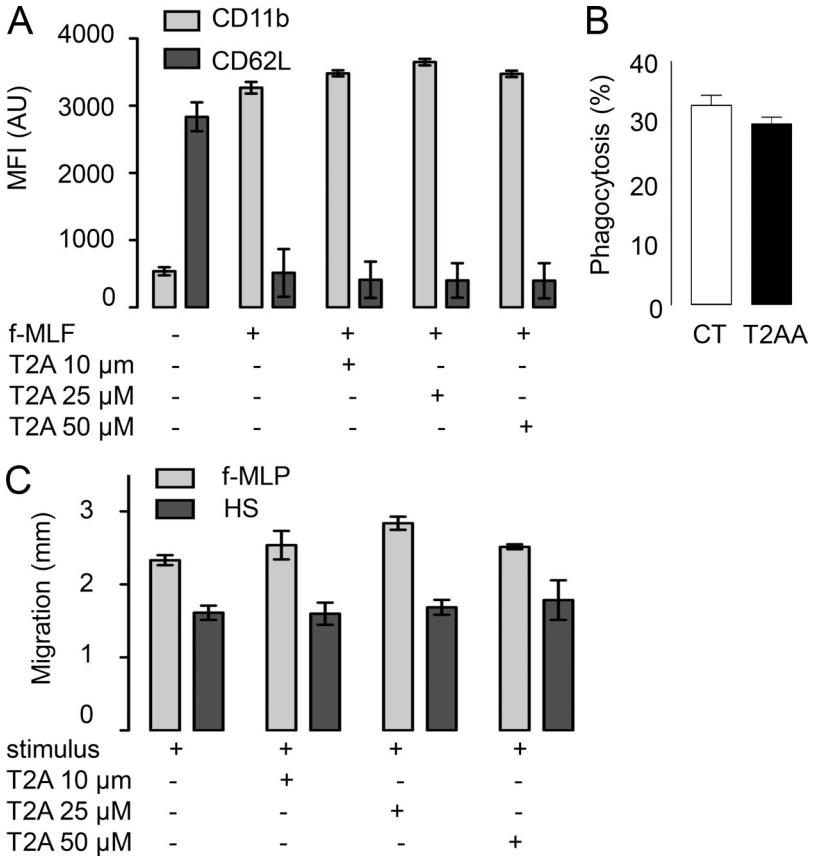


Figure S3. **Effect of T2AA on degranulation, chemotaxis, and phagocytosis in isolated human neutrophils. (A)** Evaluation of degranulation by CD11b and CD62L expression. After 30-min incubation with T2AA followed by 5-min stimulation with f-MLF (10^{-7} M), neutrophils were labeled using anti-CD11b-PE and anti-CD62L-FITC monoclonal antibodies (BD Biosciences) and analyzed by flow cytometry. The data are mean intensity of fluorescence (MFI) ± SEM; $n = 4$ different donors. **(B)** Phagocytosis of fluorescent opsonized *E. coli* by neutrophils treated or not with T2AA (50 mM) performed by flow cytometry using the IngoFlowEx Kit (Proteogenix). The data are mean ± SEM; $n = 4$. **(C)** Evaluation of chemotaxis in the response to f-MLF or C5a using migration on agarose plates as previously described (Nelson et al., 1975; Boudiaf et al., 2016). Briefly, four series of three star shapes were cut in each plate. The central well of each three-well series received 5 µl of suspension containing 10^5 neutrophils preincubated or not with different T2AA concentrations. A pool of human sera (HS) containing C5a fraction or f-MLF (10^{-7} M) was used as stimulus on first and last wells of the three-well series. Plates were incubated for 2 h at 37°C with 5% CO_2. Migration was assessed by measuring distances with an inverted microscope equipped with an ocular micrometer. No migration was observed in the absence of stimulus. The data are migration distances expressed in millimeters ± SEM; $n = 4$.

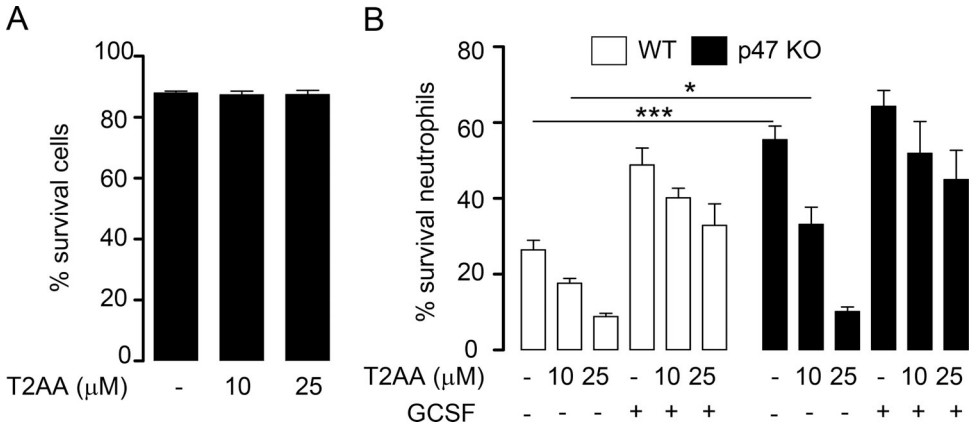


Figure S4. **Effect of T2AA on neutrophil survival isolated from WT and p47phox$^{-/-}$ mice. (A)** Effect of T2AA on bone marrow neutrophil survival. Neutrophils were isolated from bone marrow, and ex vivo spontaneous apoptosis was induced by a 16-h incubation at 37°C with or without T2AA (10–25 μM). Viable Ly6G-positive neutrophils were evaluated by flow cytometry after exclusion of Annexin-V– and 7AAD-labeled neutrophils. The data are mean ± SEM; *n* = 5 mice per group; two independent experiments. **(B)** Effect of T2AA on neutrophil survival isolated from peritoneal lavage in WT or p47phox$^{-/-}$ mice. Neutrophils were isolated from the peritoneal lavage of WT and p47phox$^{-/-}$ mice 4 h after zymosan injection and were cultured as described in A in the presence or absence of G-CSF (50 μM). Using Annexin-V and 7-AAD labeling to exclude apoptotic and necrotic neutrophils, a significant increase was observed in the percentage of surviving neutrophils from p47phox$^{-/-}$ compared with controls. G-CSF promoted survival in both control and p47phox$^{-/-}$ neutrophils, although its effect was more pronounced in controls versus p47phox$^{-/-}$. Nonetheless, T2AA decreased neutrophil survival in a dose-dependent manner in both controls and p47phox$^{-/-}$ mice in the absence or presence of G-CSF, suggesting that (i) T2AA can induce apoptosis even in the presence of G-CSF and (ii) the interaction between PCNA and p47phox was not required for PCNA prosurvival activity. The data are mean ± SEM of 13 mice (for WT) and 8 mice (for p47phox$^{-/-}$) and two independent experiments. *, P < 0.05; ***, P < 0.001, ANOVA.

Table S1. **Crystallographic data collection and refinement statistics**

Data collection statistics	**6FCM**	**6FCN**
Space group	$P2_12_12_1$	$P2_12_12_1$
Cell dimension (Å)		
a	39.18	39.88
b	140.06	140.67
c	169.97	171.77
Resolution (Å)	45.0–2.80 (2.87–2.80)	41.1–3.22 (3.30–3.22)
R_{merge} (%)[a]	4.8 (80.2)	9.6 (170.8)
Completeness (%)	97.0 (92.2)	99.4 (97.8)
I/σ	18.3 (1.62)	14.3 (1.13)
$CC_{1/2}$[b]	99.9 (71.9)	99.9 (59.0)
No. reflections	79,894 (4,753)	93,561 (6,587)
No. unique	23,289 (1,567)	16,369 (1,175)
Refinement statistics		
Protein atoms	5,790	5,784
Water	8	7
Resolution (Å)	45.0–2.80	41.1–3.22
R_{factor} (%)[c]	19.9	21.2
R_{work} (%)[c]	19.5 (35.9)	20.9 (42.5)
R_{free} (%)[c]	27.6 (38.5)	27.2 (42.6)
Rms deviations from ideality		
Bond lengths (Å)	0.008	0.007
Bond angles (°)	1.31	1.233

Values in parentheses refer to the highest-resolution shell.
[a]$R_{merge} = \Sigma_{hkl}\Sigma_i|I_i(hkl) - \langle I(hkl)\rangle|/\Sigma_{hkl}\Sigma_i I_i(hkl)$.
[b]$CC_{1/2}$ is the correlation coefficient of average intensities calculated from two random half of the measurements for each unique reflection.
[c]$R = \Sigma_{hkl}|F_{obs}(hkl) - F_{calc}(hkl)|/\Sigma_{hkl}F_{obs}(hkl)$. R_{factor} is calculated on all reflection, R_{free} on free set reflections (5% of all reflections).

References

Boudiaf, K., M. Hurtado-Nedelec, S.A. Belambri, J.C. Marie, Y. Derradji, M. Benboubetra, J. El-Benna, and P.M. Dang. 2016. Thymoquinone strongly inhibits fMLF-induced neutrophil functions and exhibits anti-inflammatory properties in vivo. *Biochem. Pharmacol.* 104:62–73. https://doi.org/10.1016/j.bcp.2016.01.006

Nelson, R.D., P.G. Quie, and R.L. Simmons. 1975. Chemotaxis under agarose: a new and simple method for measuring chemotaxis and spontaneous migration of human polymorphonuclear leukocytes and monocytes. *J. Immunol.* 115:1650–1656.